Autonomous Roll Control in a Cross-Form Rudder Submarine Using PID Controllers

Karine Chen

A thesis submitted in partial fulfillment of the requirements for the degree of

Master of Science in Aeronautics & Astronautics

University of Washington

2020

Committee:

Kristi A. Morgansen

Samuel A. Burden

Program Authorized to Offer Degree:
Aeronautics and Astronautics

University of Washington

Abstract

Autonomous Roll Control in a Cross-Form Rudder Submarine Using PID Controllers

Karine Chen

Chair of the Supervisory Committee:

When traveling on a flat, two-dimensional plane, an automobile can be considered a rigid body. However, in a three-dimensional plane, the trajectory of an underwater vehicle is more analogous to those of aircrafts. The addition of an extra dimension makes maneuverability more challenging, necessitating proper fuel consumption. Also, the third dimension creates an induced roll while turning underwater in transit from point to point, which disturbs vehicle orientation. Serving as this project's motivation, these conditions describe inefficiencies in the prevailing modus operandi. By controlling the watercraft's roll, the pilot's controls can be simplified, while also decreasing distance needed to reach the end point. This thesis describes the development of a cost-efficient standalone system, capable of both position and orientation tracking, as well as autonomous port and starboard control of a human-powered submarine (HPS). The innovation is that the primary inputs to this controller are obtained from a microcontroller outputting data from the vehicle and calculated on a PID controller using live stream data. The customized PID controller developed through the means described in this thesis utilizes a cascade control architecture to achieve horizontal stability and minimize roll motion.

ACKNOWLEDGMENTS

Foremost, I would like to express my sincere gratitude to my advisor, Kristi Morgansen, and my committee member, Samuel Burden, for their continuous support of my M.S. study and research, for their guidance, patience, and extensive knowledge. I am also immensely grateful to Eric Jones, Nicholas Valladarez, Joseph Reck, and Benjamin Maurer, all of whom provided their encouragement, insightful comments, and expertise that greatly assisted the research. This research opportunity would not have been possible without the support from the Department of Aeronautics and Astronautics Engineering, Department of Electrical and Computer Engineering (ECE), and sponsor Booz Allen Hamilton. In addition, I would like to express my appreciation towards the ECE Capstone and the UW Human-Powered Submarine team, for their collaborative efforts and providing the necessary data. Many thanks to my current and past labmates in the Nonlinear Dynamics and Control Lab, for making the lab an exciting place to work and engage in meaningful discussions. Last but not least, I would like to thank my family and friends, especially my grandma, my brother Kenny Chen, Albert Ng, David Thompson, Yu-En Yen, Min Cong Huang, and Hilda Lin, for their tremendous support.

DEDICATION

...in memory of Mary Park Christie, without whom this work would have never come to be.

TABLE OF CONTENTS

Page

List of Figures iii

List of Tables v

Nomenclature vi

Chapter 1: Introduction 1
1.1 Motivation 1
1.2 Background 3
1.3 Contributions 5
1.4 Thesis Organization 5

Chapter 2: Overall System Architecture 6
2.1 Hardware 6
2.2 Software 17

Chapter 3: Mathematical Preliminaries 19
3.1 Nonlinear Equations of Motion 19
3.2 Aerodynamics vs Hydrodynamics 19
3.3 Equations of Motion of an Aerodynamic Vehicle 20
3.4 Ship Dynamics 24
3.5 Aircraft vs HPS Control 25
3.6 Partially Submerged Submarine 25
3.7 Fully Submerged Submarine 26
3.8 Submarine Kinematic Relations 28
3.9 External Forces and Moments 29
3.10 Summation of Forces in the Roll-Axis 31

3.11 Equation of Motion in the Roll-Axis 31
3.12 Roll, Pitch, and Yaw Motions with Gravity Vector 32
3.13 Roll Dynamics 33
3.14 Added Mass 35

Chapter 4: Technical Discussion 42
4.1 Arduino Test 42
4.2 Pilot Input 46
4.3 Route Tracking Analysis 47
4.4 Control Loop Analysis 48
4.5 Constraint Analysis 52
4.6 PID Controller vs Control Surfaces 54

Chapter 5: Final Remarks 55
5.1 Work Summary 55
5.2 Future Work 56

Bibliography 63

LIST OF FIGURES

Figure Number		Page
1.1	Wire diagram of the first UW HPS in 1989.	2
1.2	Intended PID Control Loop	4
2.1	The Underdawg	6
2.2	General layout of the major system assemblies in *The Underdawg*	7
2.3	The Underdawg Hull Airfoil Selection	9
2.4	The Underdawg Rudder Airfoil Selection	9
2.5	CAD Dimensions of the HPS Rudder	10
2.6	Orientation Display of an Arduino Nano 33 IoT	12
2.7	Isometric view of the UUV surrogate (Blue Robotics).	13
2.8	Exploded view of the UUV surrogate (Blue Robotics).	14
2.9	UUV surrogate annotated	15
2.10	Pelican 1520 Case	16
2.11	Logitech F310 Gamepad	17
2.12	Mock Input Settings	17
3.1	Reference frames and ship motions.	23
3.2	Nautical terms of a watercraft	30
4.1	Arduino Prior to Calibration	43
4.2	Arduino Calibrated	43
4.3	Initial Arduino Sensor Output	44
4.4	Pilot Input via Logitech F310 Gamepad	46
4.5	Pilot Input via Simulink	46
4.6	Vehicle Trajectory Over Time	47
4.7	Longitude vs Latitude of Vehicle Trajectory	48
4.8	Typical PID Control Loop	49
4.9	Simplified PID Control Loop	49

4.10 PID Control Loop in Detail 50
4.11 Bode Plot of PID Controller 51
4.12 Bode Plot of PI Controller 52
4.13 Actuator Constraint 52
4.14 Output Constraint 53
4.15 Vehicle Horizontal Stability vs Control Surface Fin Deflection 54
5.1 Visualization of the Autonomous Roll Control 56
5.2 The bigger picture from this project 57

LIST OF TABLES

Table Number		Page
1	Definition of Abbreviations	vi
2	Definition of Variables	vi
2.1	The Underdawg Parameters	7
2.2	Centroids for The Underdawg	8
2.3	Rudder Mass Properties	11
2.4	Mass Measurements of the Standalone System	15
2.5	Cost Calculations of the Standalone System	15
3.1	Watercraft notations of forces, moments, velocities, and pose.	23
3.2	Hull Added Mass Initial Calculations	38
3.3	Hull Added Mass Coefficients	39
3.4	Rudder Added Mass Initial Calculations	41
3.5	Rudder Added Mass Coefficients	41

NOMENCLATURE

Table 1: Definition of Abbreviations

Term	**Description**
A&A	Aeronautics and Astronautics
BAH	Booz Allen Hamilton
ECE	Electrical and Computer Engineering
EOM	equations of motion
HPS	Human-Powered Submarine
IMU	inertial measurement unit
NDCL	Nonlinear Dynamics and Control Lab
RC	remote control
UUV	unmanned underwater vehicle
UW	University of Washington

Table 2: Definition of Variables

Symbol	**Description**
x,y,z	position body axes
I_x, I_y, I_z	moments of inertia about x,y,z-axes
I_{xy}, I_{yz}, I_{zx}	products of inertia about x,y,z-axes
u,v,w	linear velocity components w.r.t. body frame
Continued on next page	

Table 2 – continued from previous page

Symbol	Description
p,q,r	body-fixed angular velocities
ϕ, θ, ψ	Euler angles (roll, pitch, yaw)
$\dot{\phi}, \dot{\theta}, \dot{\psi}$	rate of change of the Euler angles
X,Y,Z	force components in body frame
L, M, N	moment components
δ_{ep}	elevator angle, port
δ_{es}	elevator angle, starboard
ρ	density of fluid
$\bar{g}$	gravitational force
ν	speed of vehicle
m	mass of vehicle
W	weight of vehicle
V	volume of water displaced
L	length of vehicle
CB	center of buoyancy
CG	center of gravity
CM	center of mass
$\bar{r}_{CB}$	position of center of buoyancy
$\bar{r}_{CG}$	position of center of gravity
x_b	position in x-axis via body frame
y_b	position in y-axis via body frame
z_b	position in z-axis via body frame
w_b	velocity in z-axis via body frame

Continued on next page

Table 2 – continued from previous page

Symbol	Description
x_g	coordinates of the center of gravity in x-axis relative to center of buoyancy
z_g	coordinates of the center of gravity in z-axis relative to center of buoyancy
x_{CB},y_{CB},z_{CB}	coordinates of CB
x_{CG},y_{CG},z_{CG}	coordinates of CG
x_B,y_B,z_B	in reference to buoyancy
x_G,y_G,z_G	in reference to gravity
F	force vector (X,Y,Z)
$\vec{F}_{TOT}$	total force
μ	moment vector (L,M,N)
μ_o	moment about the origin
$\mathbf{v}$	linear velocity (u,v,w)
$\boldsymbol{\omega}$	angular velocity vector (p,q,r)
$\mathbf{r}$	position (x,y,z)
$\boldsymbol{\theta}^T$	orientation (Euler angles: ϕ, θ, ψ)
$\mathbf{v}$	velocity
α	angle of attack (AoA)
β	sideslip angle
M_a	added mass matrix
$M_{a,hull}$	added mass matrix of the hull
$M_{a,prop}$	added mass matrix of the propeller
r_1	longitudinal radius of the hull

Continued on next page

Table 2 – continued from previous page

Symbol	Description
r_2	radius of the hull
r_{hull}	hull radius over vehicle length
k_1	one of the Lambs k-factors
ϱ	constant describing the relative proportions of the hull
c	chord of the control surface
b	span of the control surface
t	thickness of the control surface
S	surface area of the rudder
AR	aspect ratio
k_{trans}	added inertia in translation
k_{rot}	added inertia in rotation
$CB_{rudder,x}$	center of buoyancy of the rudder in the x-direction
$CB_{rudder,y}$	center of buoyancy of the rudder in the y-direction
	end of table

Chapter 1
INTRODUCTION

In general, we usually only move in two degrees of freedom, in other words, we move in two directions, either forward and backwards or left and right. When we move in an aircraft or watercraft, we add a third degree of freedom, the ability to move up and down. Vehicles maneuvering in the three-dimensional space may require its movements to be held accountable based on movements from another dimension (i.e. roll and yaw). The capability of mitigating a vehicle from 3D to 2D can reduce the pilot load and simplify the amount of manipulation required for the vehicle to get from one point to the next. Roll or attitude control controls the orientation of the vehicle, essentially facilitate the trajectory into a 2D maneuver.

Human-powered submarines are smaller form of underwater vehicles with a physical pilot onboard and is suitable for providing accessible and continuous research in underwater vehicles. Using a human-powered submarine, we can extend into more in-depth watercraft research, such as attitude control. In addition to the graphical outputs we receive from the system, we can also gain insight from the pilot onboard.

1.1 Motivation

Human-powered submarines have been been around for a long time. Examples, such as the *Turtle* and the *Hunley*, are human-powered submarines used during the Revolutionary War and Civil War, respectively [1]. Over the years, the use of human-powered submarines have slowly migrated from real world applications into student-based competitions.

Students from UW first started competing in the human-powered submarine races

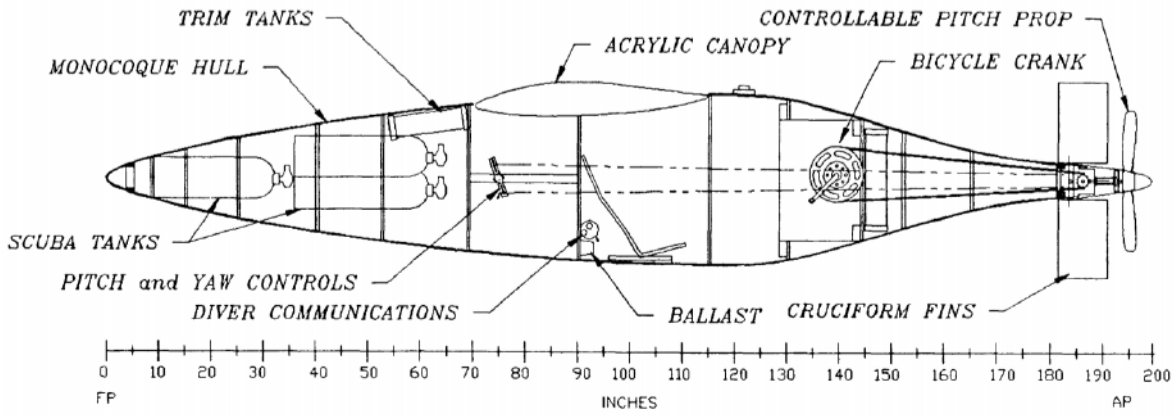

Figure 1.1: Wire diagram of the first UW HPS in 1989.

in 1989, starting with wood and eventually using foam, plastics, carbon fiber, and other composite materials for its hull [2]. The engineers can get creative designing and constructing the vehicle components as long as it is well within the competition requirements. Depending on each competition, some of the rule sets may vary, however there are some general rules that remains the same. For most competitions, the submarine must be capable of turning at top speed while maintaining a 25 m radius turn for at least 180° and maneuver between slalom poles without compromising the stability of the submarine.

Due to its impracticality and the amount of difficulties one presents, it is virtually nonexistent out in the real world. However, it is precisely this reason, which draws engineers all over the world to compete in developing the best human-powered submarine in a controlled competition. Though human-powered submarine are unrealistic to use in general world applications, it is still extremely valuable, as it contributes to engineering research and provides a great exercise to prepare students into the working field. This example provides a comprehensive understanding and analytical methods in engineering problem solving.

In addition to the HPS vehicles, there is an increase in technological advance-

ment in underwater vehicles. With the improvement in processing capabilities and high yield components, unmanned underwater vehicles (UUV) are given additional roles and tasks. In addition to military advancement underwater, the usage of underwater vehicles also encourage deep sea exploration and studies in aquatic science and oceanography. Open waters can be a dangerous place. Researchers use UUVs to study rivers, lakes, ocean, and even in-depth down to the ocean floors. Utilizing UUVs provide a safety net, allowing people to remain in a safe environment while conducting the same research. Therefore, research to further expand the capabilities of underwater vehicles is crucial.

This thesis investigates in developing a cost efficient standalone system (limited by physical constraint), capable of position tracking and autonomous roll control using a PID controller with a cascade control architecture.

1.2 Background

Constant strive in improving the capability of a human-powered submarine has been a goal for college engineers on a global scale. Most of the research conducted involve enhancing the physical hardware itself, however, we can investigate reducing pilot work load utilizing autonomous control. Since we are dealing with an underwater vehicle that fills up with water under water, it is helpful to develop an electronics system capable of attitude control contained in a watertight vessel.

1.2.1 Autonomous Control

One of the first challenges involving a human-powered submarine is to maintain a set trajectory relying on the pilot's sight while maneuvering. Pilots are limited to the forward-facing view and still required to manipulate the rudders and elevators while thrusting the vehicle. 3D maneuvers can disorient the vehicle and create even more problems on attempting to maintain a straight trajectory. Thus, designing a system to automatically control the vehicle's local horizontal attitude would alleviate some

of the pilot's agenda, so the pilot would only need to focus in the 2D plane.

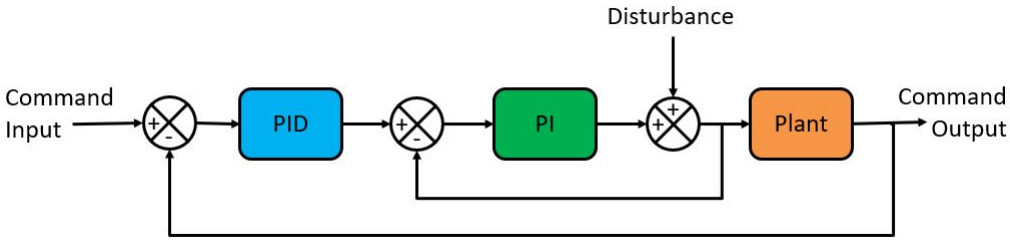

Figure 1.2: Intended PID Control Loop

1.2.2 Physical Constraint

The human-powered submarine is also limited by its physical constraint. In order to increase vehicle maneuverability and speed, it requires the entire system to be as consolidated as it can be. Since the vehicle hosts a human pilot in addition to the hardware involved in the assembly, there isn't a whole lot of room to add more components. Therefore, this requires the roll control hardware to be as minuscule as it can be.

1.2.3 Standalone System

The objective of this project is to first develop an attitude controller, implement the controllers into the UUV Surrogate, then into the human-powered submarine. The underlying goal would be to be able to integrate this system into other vehicles, including unmanned underwater vehicles. Since the ultimate goal of this roll control hardware is the integration capability for a submarine out in the open waters, it also needs to be a standalone control system, which can easily be switched out of each vehicle.

1.3 Contributions

Developing an autonomous roll control standalone system will reduce the pilot's work load in a human-powered submarine, making the competition more straight forward. Furthermore, this research is intended to be tested on the human-powered submarine and eventually integrated into autonomous submarines. This would add an underwater capability to the current availability of autonomous unmanned vehicles, performing variable tasks without endangering any human personnel. It could then be replicated, mass produced, and distributed to multiple vehicles at once, providing low cost efficiency to underwater exploration.

1.4 Thesis Organization

In the second chapter, we introduce the commercially available hardware and software and how it is all integrated into the system. In Chapter 3, we discuss the mathematical preliminaries behind the vehicle dynamics and justify the overall simplification to solely the roll-axis. Chapter 4 explores the process and the methods used for this project and how it all connects, along with an in depth analysis to the results compiled. Last but not least, Chapter 5 concludes this thesis with its final remarks and provides suggested future work encouraged by this effort.

Chapter 2

OVERALL SYSTEM ARCHITECTURE

In this section, we first describe both the hardware and software components that make up this system. We then move onto the connections, interaction, and function of the various pieces that make up the overall system. And lastly, we describe how everything comes together to produce an attitude controller. Detailed work utilizing the hardware and software listed below are found under Section 4.

2.1 Hardware

2.1.1 Human-Powered Submarine (HPS)

Figure 2.1: The Underdawg

The Underdawg is a human-powered submarine designed by the UWHPS team, spanning $2.72m$ long and $181.44kg$ in mass, not including the pilot. The general layout of the major system assemblies (Fig.2.2) include safety, propulsion, and controls

housed by the hull of the vehicle, and control surfaces and a propulsor is connected on the exterior.

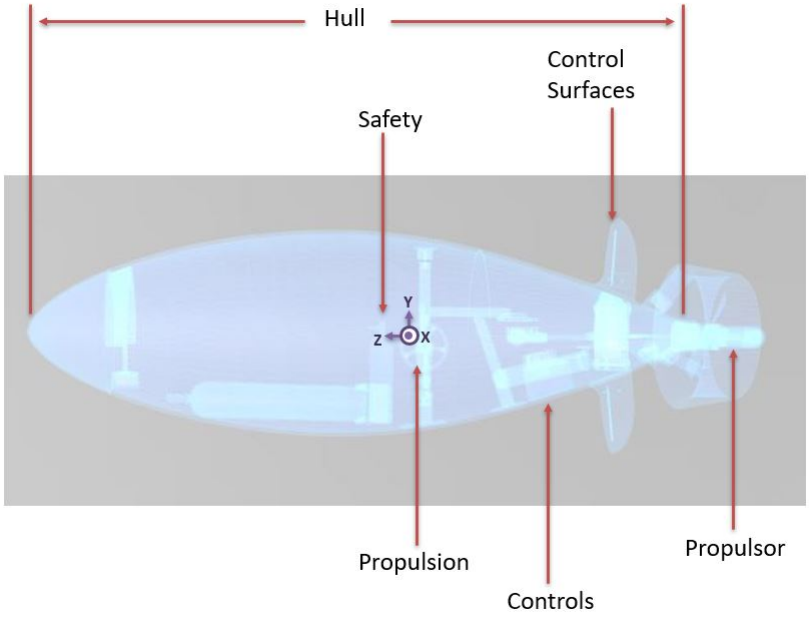

Figure 2.2: General layout of the major system assemblies in *The Underdawg*

Table 2.1: The Underdawg Parameters

Overall Length	2.72 m
Total Weight	181.44 kg
Hull Weight	56.25 kg
Contained Volume	0.406 m^3
Propulsion	Propeller
Propeller Type	2-Bladed Single Propeller

For The Underdawg to be neutrally buoyant and stable, the submarine model was first analyzed through a CAD model via Solidworks. Centroid positions were esti-

mated where the longitudinal, lateral, and vertical CG location are aft of the origin, laterally offset, and below the centerline, respectively. The vehicle ended up to be slightly positive buoyant than the calculated values with all the components installed, a common predicament discussed in Section 1. However, with the ballast method in adding additional weight to the lower quarter, vertically aligning the centroid positions, thus passively adjust for induced roll.

Table 2.2: Centroids for The Underdawg

Centroid Type	Units	x (longitudinal)	y (lateral)	z (vertical)
Center of Gravity	m	-0.224	0.0041	-0.0455
Center of Buoyancy	m	-0.0122	0.0003	-0.0089

Based on *The Underdawg* design, we know that the vehicle has rotational symmetry about the x-axis, i.e. port-starboard and top-bottom symmetry. For the purposes of this project, we only assume the vehicle as a deeply submerged body, therefore, we can assume constant added mass coefficients. Since the competition is based in a pool, we assume no waves, currents, or other disturbances, but some small random noises are added to account for the divers and pool walls surrounding the vehicle.

The airfoil selection for the hull uses two different airfoil/hydrofoil profiles for its beam and draft. The beam of the watercraft or the width of the watercraft at its widest point, uses the Eppler 520 Airfoil (e520-il) sized at $2.8m$ with a 1.2 thickness scaling factor. While the draft profile is scaled at $2.8m$ using the Eppler E838 Hydrofoil (e838-il) with a thickness scaling factor of 1.45.

The four control surfaces, i.e. rudders, uses the NACA 8000 Airfoil, which accommodates the $12.7mm$ control rod cast on the rudders while minimizing any excess material. In addition, Table 3.4 shows the rudder mass properties calculated through Solidworks.

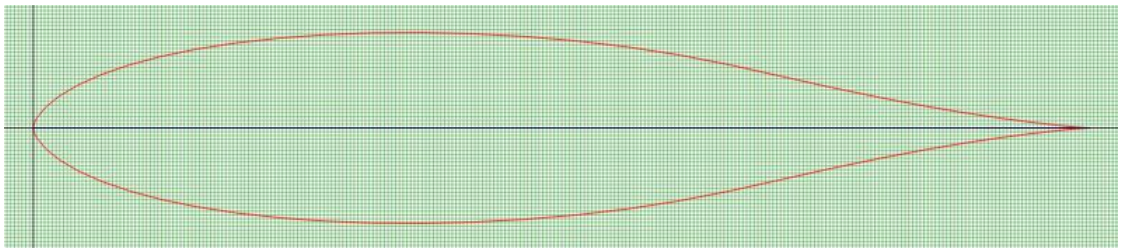

(a) Beam

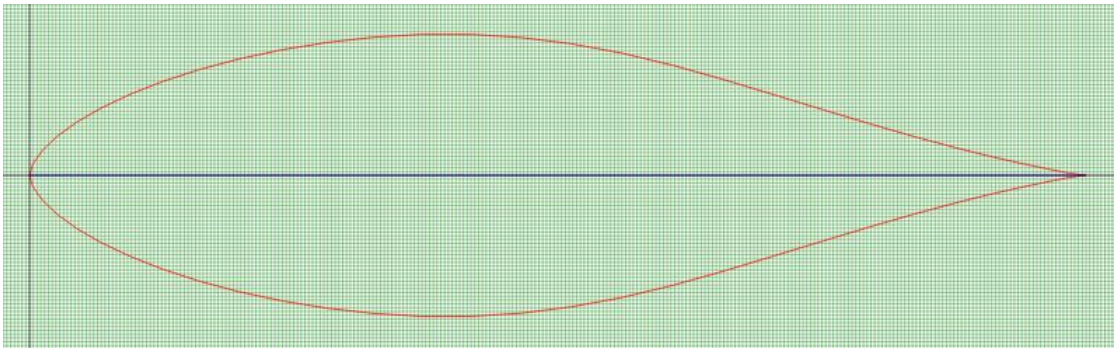

(b) Draft

Figure 2.3: The Underdawg Hull Airfoil Selection

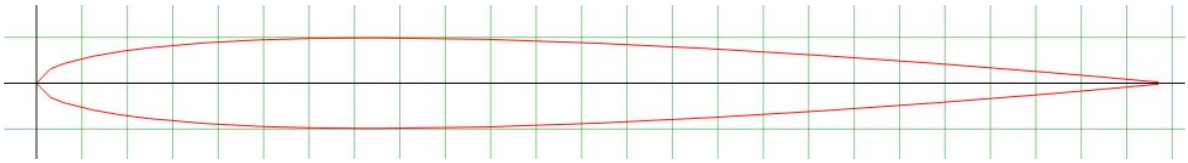

Figure 2.4: The Underdawg Rudder Airfoil Selection

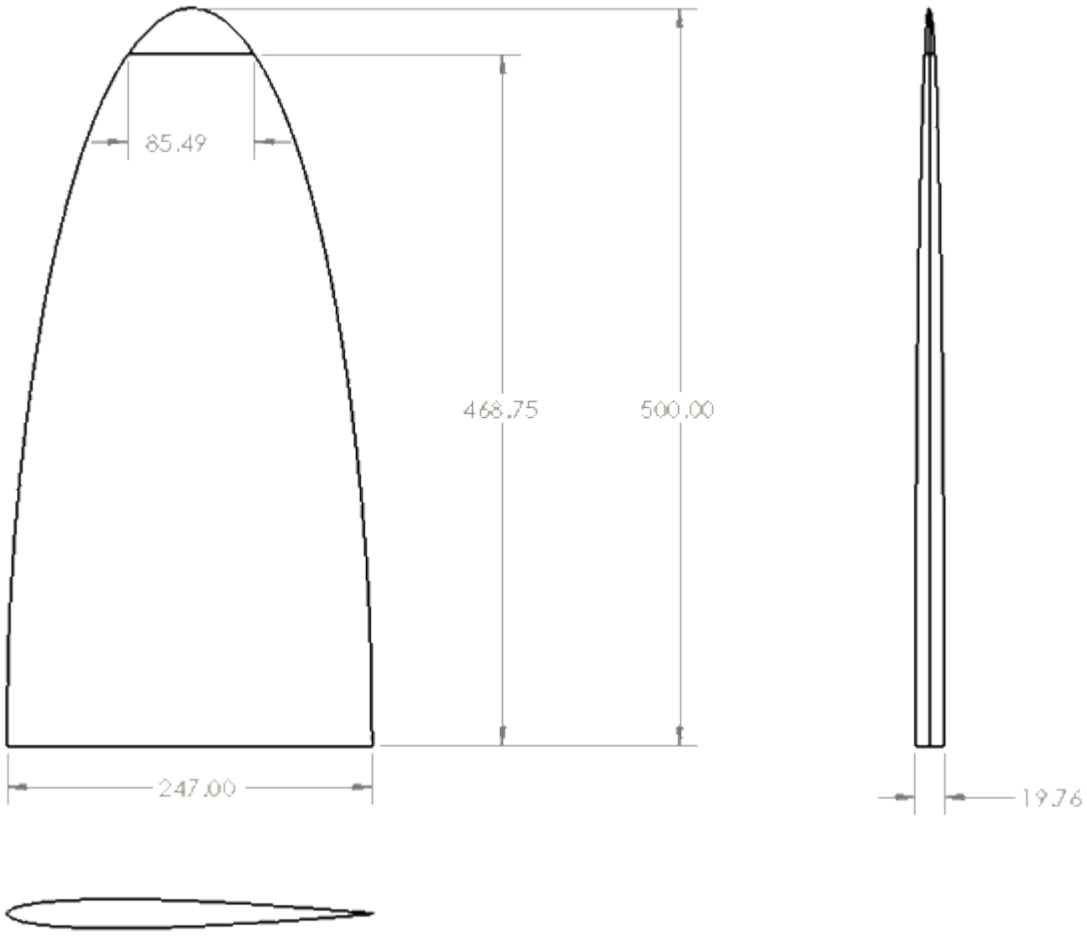

Figure 2.5: CAD Dimensions of the HPS Rudder

Table 2.3: Rudder Mass Properties

Center of Mass $[m]$		
$CM_{rudder,x} = -0.02$		
$CM_{rudder,y} = 0.00$		
$CM_{rudder,z} = 0.19$		
Principal Axes of Inertia $[kg/m^2]$		
$I_x = (0.03, 0.00, 1.00)$		
$I_y = (1.00, 0.00, -0.03)$		
$I_z = (0.00, 1.00, 0.00)$		
Principal Moments of Inertia $[kg/m^2]$		
$P_x = 0.00$		
$P_y = 0.02$		
$P_z = 0.02$		
Moments of Inertia $[kg/m^2]$		
$L_{xx} = 0.05$	$L_{xy} = 0.00$	$L_{xz} = 0.00$
$L_{yx} = 0.00$	$L_{yy} = 0.05$	$L_{yz} = 0.00$
$L_{zx} = 0.00$	$L_{zy} = 0.00$	$L_{zz} = 0.00$

2.1.2 Arduino Nano 33 IoT

The system uses an Arduino Nano 33 IoT, an Arduino with a microcontroller and onboard sensors for control navigation and environmental data, which can be outputted via direct serial, WiFi, or Bluetooth low energy (BLE) communications. This Arduino was chosen since it is low in cost, includes variable connections with serial, WiFi, and/or Bluetooth low energy (BLE) connectivity, and it is compatible with the MATLAB and Simulink software.

Components include the following: a low power Arm® Cortex®-M0 32-bit SAMD21

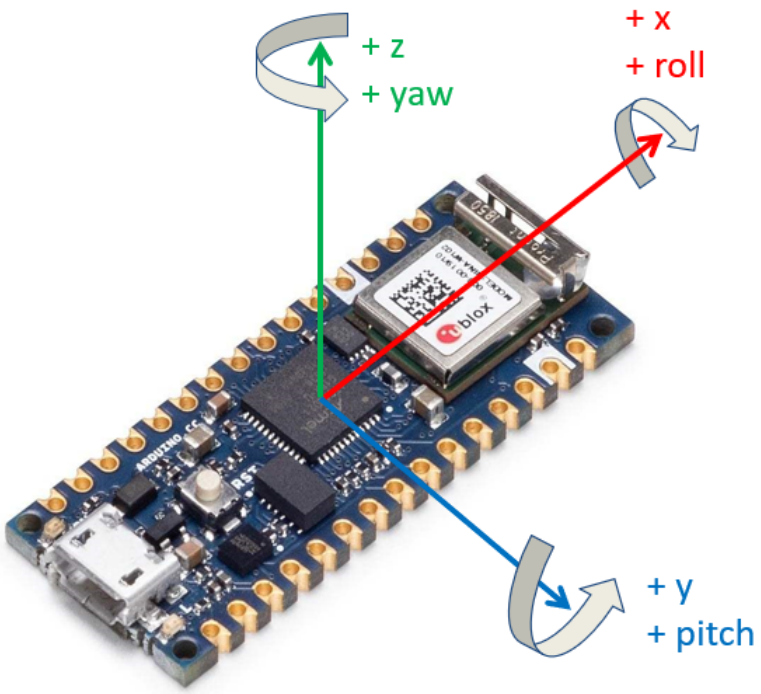

Figure 2.6: Orientation Display of an Arduino Nano 33 IoT

as its main processor, a LSM6DS3 6-axis IMU sensor, a u-blox NINA-W102 radio, and a Microchip® ECC608 crypto chip. The IMU, suitable for relative positioning,

includes a 3-axis accelerometer, measuring linear acceleration, and a 3-axis gyroscope, measuring angular velocity. The u-blox is a low power chipset, which operates at the 2.4 GHz range for WiFi and Bluetooth® connectivity. The ECC608 crypto chip can be configured and secured in its WiFi settings when the Arduino is detected in the online mode.

In terms of orientation (depicted in Fig.2.6), the x-axis goes from USB connector to Bluetooth antenna is positive, the y-axis goes from analog and power pins to digital pins is positive, and the z-axis passes through the PCB, component side upwards is positive, while going below is negative.

2.1.3 Surrogate UUV Standalone System

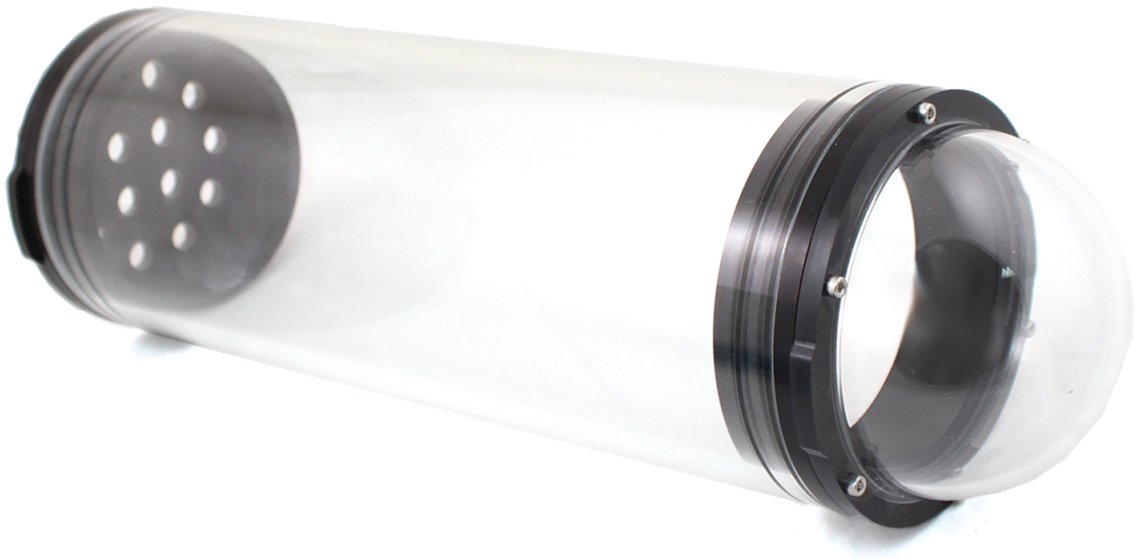

Figure 2.7: Isometric view of the UUV surrogate (Blue Robotics).

Placed inside the human-powered submarine is a standalone system, which will consist of a microcontroller and sensors inside a configurable watertight container.

The watertight enclosure, which we call the UUV surrogate (Fig.2.7), houses the Arduino Nano 33 IoT, and serves to allow independent tests to be ran without involving the human-powered submarine.

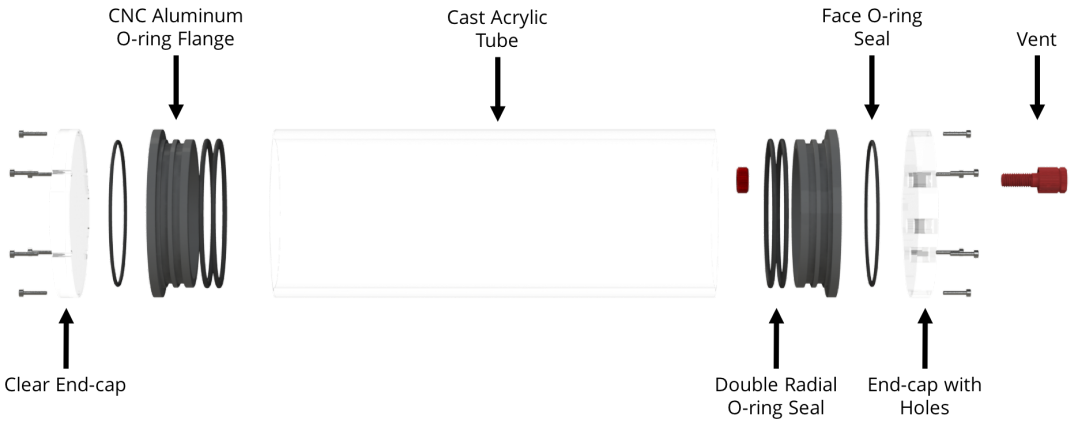

Figure 2.8: Exploded view of the UUV surrogate (Blue Robotics).

Rather than following the exact replica shown in the exploded view of the UUV surrogate (Fig.2.8), custom modifications were made to better suit the intentions of the UUV surrogate. The UUV surrogate consists of a 298m cast acrylic tube and in place of the end-cap with holes, it is replaced with a 4" series dome end cap. In addition to the clear end-cap, a clear acrylic end cap 11.5mm thick is permanently glued on to the clear end-cap to seal off the tail end completely, making it also able to stand upright. The intention for such modifications is so the container will be somewhat in the shape of a UUV and control surfaces can be attached for the UUV surrogate to maneuver itself in the water.

The clear acrylic plastic tube provides easy visibility for the components inside the enclosure and is rated to venture into depths of 100 m. Double O-ring sealed flanges prevent any water from getting inside and interchangeable end caps allow user customization.This puts the standalone system at roughly $250 in cost and $3kg$ in added mass, with miscellaneous including batteries and wiring etc.

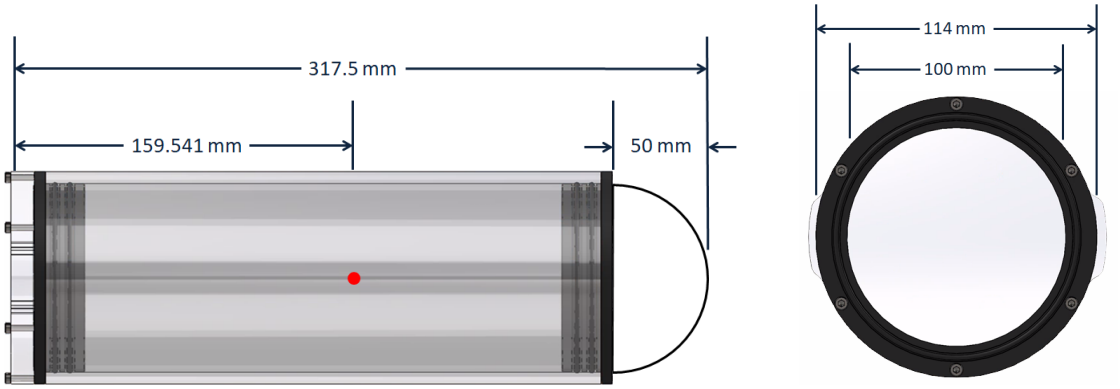

(a) Side View (b) Top View

Figure 2.9: UUV surrogate annotated

Table 2.4: Mass Measurements of the Standalone System

Component	Mass $[kg]$
UUV Surrogate	1.286
Arduino Nano 33 IoT	0.005
3D Printed Mold	$\sim$ 0.500
Miscellaneous	$\sim$ 1.209
Total Mass	$\sim$ 3.000

Table 2.5: Cost Calculations of the Standalone System

Component	Description	Cost [$]
UUV Surrogate	Houses the electronics system.	$\sim$ 200
Autopilot Hardware	Microcontroller with sensors, battery system, onboard storage.	$\sim$ 50
Software	Programs and libraries.	0
Total Cost		$\sim$ 250

2.1.4 Pelican 1520 Case

A Pelican 1520 Case (Fig.2.10), was selected to hold the UUV surrogate's form factor and protect the system from any wear and tear outside of testing. The interior is dimensioned at 458.72 x 327.41 x 170.69 mm, allowing ample room to fit the UUV surrogate and other miscellaneous items. The case comes with the Pick N'Pluck foam, easily pluckable 1/2" cubes, which allows interior customization to form fit the UUV surrogate. In addition, it has a built-in Automatic pressure Equalization Valve, suitable for keeping water out and releases any built-up air pressure. The lock also comes with stainless steel reinforced padlock protectors to ensure the case is tightly shut.

Figure 2.10: Pelican 1520 Case

2.1.5 Logitech F310 Gamepad

The Logitech F310 Gamepad (Fig.2.11) is used to mock pilot interface, with a constant velocity of $\mathbf{v} = 0.5m/s$. The control configurations are shown in Fig.2.12, where the joysticks mock the roll, pitch, yaw, and throttle of the human-powered submarine.

Figure 2.11: Logitech F310 Gamepad

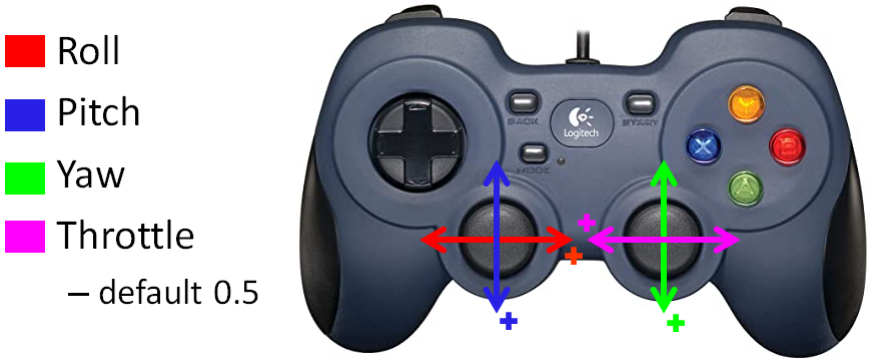

Figure 2.12: Mock Input Settings

2.2 Software

The software used for this project include the Arduino, Arduino Create, MATLAB, Simulink, and Solidworks. The desktop Arduino was used to initialize the Arduino

Nano 33 IoT and codes were created to provide sensor output values. The Arduino Create, the online web browser version of Arduino was used to validate and configure the WiFi connection. Solidworks was used to create and analyze CAD models of the human-powered submarine and the UUV Surrogate. MATLAB (version 2020a) was used to develop scripts that can be reran and also calculate various values presented in this paper.

The following MATLAB packages were used and required for this research:

- Simulink® 3D Animation™
- Aerospace Toolbox
- Aerospace Blockset
- DSP System Toolbox
- Simulink Design Optimization
- I2C block for ArduinoIO simulink package
- MinGW
- Simulink 3D Animation
- Marine Systems Simulator Toolbox (MSS toolbox)
- Marine Visualization Toolbox

The toolbox listed above are required to conduct specific experiments also found in Section 4, some of which include syncing the Logitech F310 Gamepad to override pilot controls, additional blocks used for the Simulink models, and visualization toolboxes to further validate the outputs produced.

Chapter 3

MATHEMATICAL PRELIMINARIES

In this chapter,

3.1 Nonlinear Equations of Motion

To model a human-powered submarine, we first take a look at the different states (Eq.3.1) and controls (Eq.3.2), and develop the equations needed to describe the system model. Since the vehicle will be submerged, we can assume the properties of an aerodynamic vehicle, and define the ailerons, elevator, rudder, and propulsion (thrust) to be the four controllers. Similar to other watercraft, we can can assume the vehicle to also have linear (Eq.3.3) and angular velocities (Eq.3.4) in the body-fixed reference frame.

States

$$\vec{x} \triangleq \{ \underbrace{u, v, w,}_{\text{translational}} \overbrace{p, q, r,}^{\text{rotational}} \underbrace{x, y, z,}_{\text{position}} \overbrace{\phi, \theta, \psi}^{\text{orientation}} \} \in \mathbb{R}^{12} \tag{3.1}$$

Controls

$$\vec{u} \triangleq \{\delta_{AIL}, \delta_{ELEV}, \delta_{RUDD}, \delta_{TH}\} \in \mathbb{R}^4 \tag{3.2}$$

3.2 Aerodynamics vs Hydrodynamics

In the case of a hull, completely immersed, its hydrodynamics is considered to be parallel to aerodynamics, therefore, we can use similar equations for calculation.

$$\mathbf{v} = \Big[u, v, w\Big]^T \tag{3.3}$$

$$\boldsymbol{\omega} = \Big[p, q, r\Big]^T \tag{3.4}$$

$$\mathbf{r} = \Big[x, y, z\Big]^T \tag{3.5}$$

$$\boldsymbol{\theta} = \Big[\phi, \theta, \psi\Big]^T \tag{3.6}$$

We can calculate the linear velocity

$$\begin{bmatrix} u \\ v \\ w \end{bmatrix} = \mathbf{v} \begin{bmatrix} cos(\alpha)cos(\beta) \\ sin(\beta) \\ sin(\alpha)cos(\beta) \end{bmatrix} \tag{3.7}$$

$$\begin{bmatrix} \mathbf{v} \\ \alpha \\ \beta \end{bmatrix} = \begin{bmatrix} \sqrt{u^2 + v^2 + w^2} \\ tan^{-1}(w/u) \\ sin^{-1}(v/\mathbf{v}) \end{bmatrix} \tag{3.8}$$

where

$\mathbf{v} \equiv$ velocity

$\alpha \equiv$ angle of attack (AoA)

$\beta \equiv$ sideslip angle

$$\vec{x} = \Bigg[\underbrace{u, v, w}_{\mathbf{v}} \overbrace{p, q, r,}^{\boldsymbol{\omega}} \underbrace{x, y, z,}_{\mathbf{r}} \overbrace{\phi, \theta, \psi}^{\boldsymbol{\theta}}\Bigg]^T \tag{3.9}$$

$$= \Big[\mathbf{v}^T \boldsymbol{\omega}^T \mathbf{r}^T \boldsymbol{\theta}^T\Big]^T \tag{3.10}$$

From there, we can then get a straight and level state vector:

$$\vec{x}^* = \Big[\ \mathbf{v}cos(\varrho) \quad 0 \quad \mathbf{v}sin(\varrho) \quad 0 \quad 0 \quad 0 \quad x_0 \quad y_0 \quad z_0 \quad 0 \quad \theta_0 \quad 0\ \Big]^T \tag{3.11}$$

3.3 Equations of Motion of an Aerodynamic Vehicle

As deduced earlier, we can use similar components of an aerodynamic system for a hydrodynamic system as long as the watercraft is submerged.

3.3.1 Force Components in the Body Frame

First, we take a look at the equations of motion on the force components in a body frame.

$$\sum \vec{F} = \vec{f}_{AERO} + \vec{f}_{PROP} + \vec{f}_{GRAV} \tag{3.12}$$

$$= m(\dot{\mathbf{v}}_b + \boldsymbol{\omega} + \mathbf{v}_b) \tag{3.13}$$

$$= m\left(\begin{bmatrix} \dot{u} \\ \dot{v} \\ \dot{w} \end{bmatrix} + \underbrace{\begin{bmatrix} p \\ q \\ r \end{bmatrix} \times \begin{bmatrix} u \\ v \\ w \end{bmatrix}}_{\begin{bmatrix} \hat{x}_b & \hat{y}_b & \hat{z}_b \\ p & q & r \\ u & v & w \end{bmatrix}} \right) \tag{3.14}$$

$$= m \begin{bmatrix} \dot{u} \\ \dot{v} \\ \dot{w} \end{bmatrix} + mdet \begin{bmatrix} \hat{x}_b & \hat{y}_b & \hat{z}_b \\ p & q & r \\ u & v & w \end{bmatrix} \tag{3.15}$$

$$= m \begin{bmatrix} \dot{u} + qw - rv \\ \dot{v} + ru - pw \\ \dot{w} + pv - qu \end{bmatrix} = \begin{matrix} \sum X \\ \sum Y \\ \sum Z \end{matrix} \tag{3.16}$$

$$\vec{f}_{GRAV} = R_1(\phi)R_2(\theta) \begin{pmatrix} 0 \\ 0 \\ \bar{g} \end{pmatrix} \tag{3.17}$$

$$= \begin{bmatrix} -\bar{g}sin(\theta) \\ \bar{g}sin(\phi)cos(\theta) \\ \bar{g}cos(\phi)cos(\theta) \end{bmatrix} \tag{3.18}$$

3.3.2 Moment Components in the Body Frame

Next, we can take a look at the equations of motion on the moment components (rotational acceleration) in a body frame.

$$\sum \mu = \begin{Bmatrix} \sum L \\ \sum M \\ \sum N \end{Bmatrix} \tag{3.19}$$

Here, we set $\dot{I} = 0$:

$$\sum \mu = \frac{\delta}{\delta t}(I\boldsymbol{\omega}) + \boldsymbol{\omega} \times (I\boldsymbol{\omega}) \tag{3.20}$$

$$= \underbrace{I \begin{Bmatrix} \dot{p} \\ \dot{q} \\ \dot{r} \end{Bmatrix}}_{\frac{\delta}{\delta t}(I\boldsymbol{\omega})} + \begin{Bmatrix} p \\ q \\ r \end{Bmatrix} \times I \begin{Bmatrix} p \\ q \\ r \end{Bmatrix} \tag{3.21}$$

By symmetry, $I_{xy} \equiv I_{yz} \equiv 0$ in the inertia tensor I (Eq.3.22), resulting in Eq.3.23.

$$I \triangleq \begin{bmatrix} I_x & -I_{xy} & -I_{xz} \\ -I_{xy} & I_y & -I_{yz} \\ -I_{xz} & -I_{yz} & I_z \end{bmatrix} \tag{3.22}$$

$$= \begin{bmatrix} I_x & 0 & -I_{xz} \\ 0 & I_y & 0 \\ -I_{xz} & 0 & I_z \end{bmatrix} \tag{3.23}$$

Note: $I_x \equiv I_{xx}$, $I_y \equiv I_{yy}$, and $I_z \equiv I_{zz}$.

$$\therefore \begin{bmatrix} L \\ M \\ N \end{bmatrix} = \begin{bmatrix} I_x\dot{p} - I_{xz}\dot{r} - qpI_{xz} + qrI_z - rqI_y \\ I_y\dot{q} + p^2I_{xz} - prI_z + rpI_x - r^2I_{xz} \\ -I_{xz}\dot{p} + I_z\dot{r} + pqI_y - qpI_xqrI_{xz} \end{bmatrix} \tag{3.24}$$

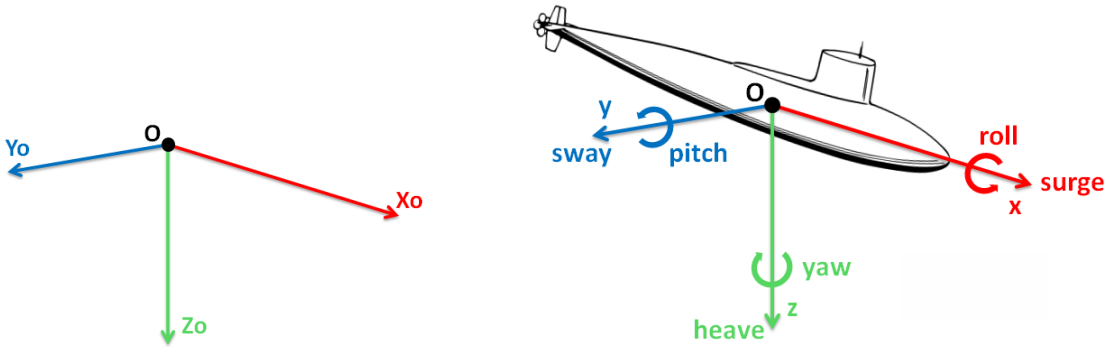

(a) Earth-Fixed (b) Body-Fixed

Figure 3.1: Reference frames and ship motions.

Table 3.1: Watercraft notations of forces, moments, velocities, and pose.

DOF #	**Motion**	**Forces & Moments**	**Linear & Angular Velocities**	**Pose**
1	Surge	X	u	x
2	Sway	Y	v	y
3	Heave	Z	w	z
4	Roll	L	p	ϕ
5	Pitch	M	q	θ
6	Yaw	N	r	ψ

3.4 Ship Dynamics

We can split the 12 states (Eq.3.1) into two different reference frames, with the possible six motions of a watercraft shown in Fig.3.1. In the earth-fixed frame (O, X_o, Y_o, Z_o), the positions and Euler angles of the vehicle are denoted as x, y, z and ϕ, θ, ψ. While in the body-fixed frame (o, x, y, z), the vehicle's linear and angular velocities are denoted as u, v, w (surge, sway, and heave) and p, q, r (roll, pitch, and yaw).

Linear and Angular Velocities (via Body-Fixed Reference Frame)

$$\vec{v} = \Big[u, v, w, p, q, r\Big]^T \tag{3.25}$$

Position and Orientation (Euler) Angles (via Earth-Fixed Reference Frame)

$$\vec{\zeta} = \Big[x, y, z, \phi, \theta, \psi\Big]^T \tag{3.26}$$

Mapping Between Position and Orientation and Velocities

$$\dot{\zeta} = J(\zeta)\vec{v} \tag{3.27}$$

Nonlinear Equations of HPS (in Compact Form)

$$m\dot{\vec{v}} + C(\vec{v})\vec{v} + D(\vec{v})\vec{v} + g(\zeta) = \tau \tag{3.28}$$

where

$$\begin{aligned} m\dot{\vec{v}} &\equiv 6 \times 6 \text{ inertia matrix} \\ C(\vec{v}) &\equiv \text{matrix of Coriolis and centripetal force terms} \\ D(\vec{v} &\equiv \text{damping matrix} \\ g(\zeta) &\equiv \text{gravitational forces and moments vector} \\ \tau &\equiv \text{control inputs vector} \end{aligned}$$

Matrices $m\dot{\vec{v}}$ and $C(\vec{v})$ both includes the added mass calculations. And we call the matrix C, the Coriolis matrix, and $C(\vec{v})$ gives the Coriolis and centrifugal force terms.

3.5 Aircraft vs HPS Control

We first take a look at the controls in an aircraft vs a submarine (specific to the HPS vehicle). Even though we are given two elevator control and two rudder control, the pilot will have command to override the autonomous control. The autonomous control will only have control over the two elevator controls (starboard and port), but these will be somewhat coupled.

Aircraft Control

$$\bar{u}^* = \begin{bmatrix} \delta E_0 & \delta A_0 & \delta R_0 & \delta T_0 \end{bmatrix}^T$$

where

$$E \equiv \text{elevator angle}$$

$$A \equiv \text{aileron angle}$$

$$R \equiv \text{rudder angle}$$

$$T \equiv \text{thrust}$$

Submarine (HPS) Control

$$\bar{u}^* = \begin{bmatrix} \delta E_0 & \delta R_0 \end{bmatrix}^T$$

where

$$E \equiv \text{diving plane / hydroplane angle}$$

$$R \equiv \text{rudder angle (steering left and right)}$$

3.6 Partially Submerged Submarine

In a partially submerged submarine, the total force due to gravitational and buoyancy effects is depicted in Eq.3.29 and the moment about the origin is in Eq.3.30. However, since the electronics in the submarine will not start until the vehicle is in the water,

and the autonomous control when it is fully submerged, we can neglect the forces and moments when the submarine is only partially submerged.

$$\vec{F}_{TOT} = m\bar{g} - \rho V\bar{g} \tag{3.29}$$

where

$\bar{g} \equiv$ gravity vector

$m \equiv$ mass of vehicle

$\rho \equiv$ density of fluid

$V \equiv$ volume of vehicle or water displaced

$$\mu_o = m\bar{r}_{CG} \times \bar{g} - \rho V\bar{r}_{CB} \times \bar{g} \tag{3.30}$$

where

$\bar{g} \equiv$ gravity vector

$m \equiv$ mass of vehicle

$\rho \equiv$ density of fluid

$V \equiv$ volume of vehicle or water displaced

$\bar{r}_{CB} \equiv$ position of center of buoyancy

$\bar{r}_{CG} \equiv$ position of center of gravity

3.7 Fully Submerged Submarine

When the submarine is fully submerged, we can assume that it is neutrally buoyant. We can assume that the mass of the vehicle will be the density of fluid multiplied by the volume of the vehicle. In the case of the human-powered submarine, when the vehicle is fully submerged, the interior is filled up with water, and therefore, the volume of the vehicle also includes the water being displaced.

$$m = \rho V \tag{3.31}$$

where

$$m \equiv \text{mass of vehicle}$$

$$\rho \equiv \text{density of fluid}$$

$$V \equiv \text{volume of vehicle}$$

Even though there is no linear force as shown in Eq.3.31, there is a turning moment, so the moment about the origin will be as shown in Eq.3.32. Note that the moment about the origin is the same fully submerged as it is when it is partially submerged.

$$\mu_o = m\bar{r}_{CG} \times \bar{g} - \rho V \bar{r}_{CB} \times \bar{g} \tag{3.32}$$

where

$$\bar{g} \equiv \text{gravity vector}$$

$$m \equiv \text{mass of vehicle}$$

$$\rho \equiv \text{density of fluid}$$

$$V \equiv \text{volume of vehicle or water displaced}$$

$$\bar{r}_{CB} \equiv \text{position of center of buoyancy}$$

$$\bar{r}_{CG} \equiv \text{position of center of gravity}$$

One of the features about a submarine is that the position of the center of gravity and center of buoyancy in the y-axis will always be the same, and it is the same case for the human-powered submarine. Therefore, we can neglect the y-components of both the $\bar{r}_{CG}$ and $\bar{r}_{CB}$.

$$\bar{r}_{CG} = \begin{bmatrix} x_{CG} \\ 0 \\ z_{CG} \end{bmatrix} \tag{3.33}$$

$$\bar{r}_{CB} = \begin{bmatrix} x_{CB} \\ 0 \\ z_{CB} \end{bmatrix} \tag{3.34}$$

Because of the neutral buoyancy condition equation of a neutrally buoyant submarine (Eq.3.31, we can eliminate ρV from the moment equation (Eq.3.32), then:

$$\mu_o = m(\bar{r}_{CG} - \bar{r}_{CB}) \times \bar{g} \tag{3.35}$$

Furthermore, if we substitute $\bar{r}_{CG}$, $\bar{r}_{CB}$, and $\bar{g}$, we can show that the moment of gravitational and buoyancy forces can be approximated for small roll and pitch angles by:

$$\mu_o = -mg(z_{CG} - z_{CB}) \begin{bmatrix} \phi \\ \theta \\ 0 \end{bmatrix} - mg(x_{CG} - x_{CB}) \begin{bmatrix} 0 \\ 1 \\ -\phi \end{bmatrix} \tag{3.36}$$

Specific to the human-powered submarine, we are given that $x_{CG} = x_{CB}$ holds. Since a stable state is required to linearize about and we are able to fulfill said condition, we can deduce the moment about the origin to the following equation:

$$\mu_o = -mg(z_{CG} - z_{CB}) \begin{bmatrix} \phi \\ \theta \\ 0 \end{bmatrix} \tag{3.37}$$

3.8 Submarine Kinematic Relations

The kinematic relations of a submarine [3] can be depicted as follows:

$$\dot{\phi} = p + \dot{\psi} sin(\theta) \tag{3.38}$$

$$\dot{\theta} = \frac{g - \dot{\psi} cos(\theta) sin(\phi)}{cos(\theta)} \tag{3.39}$$

$$\dot{\psi} = \frac{r + \theta sin(\phi)}{cos(\theta)cos(\phi)} \tag{3.40}$$

Same as the kinematics of an aerodynamic vehicle, we can simplify the vectors, which holds true for small angles of movement.

For simplification, set:

$$\begin{bmatrix} \dot{\phi} & \dot{\theta} & \dot{\psi} \end{bmatrix}^T = \begin{bmatrix} p & q & r \end{bmatrix}^T \tag{3.41}$$

3.9 External Forces and Moments

In addition, we have to account for the external forces and moments acting on the hydrodynamic vehicle.

$$\sum F_{EXT} = \vec{F}_{HYDRO} + \vec{F}_{LIFT} + \vec{F}_{DRAG} + \vec{F}_{CTRL} + \vec{F}_{NOISE} \tag{3.42}$$

where

$$\begin{aligned} \textstyle\sum F_{EXT} &\equiv \text{external forces} \\ \textstyle\sum F_{HYDRO} &\equiv \text{hydrostatic forces} \\ \textstyle\sum F_{LIFT} &\equiv \text{lift forces} \\ \textstyle\sum F_{DRAG} &\equiv \text{drag forces} \\ \textstyle\sum F_{CTRL} &\equiv \text{control forces} \\ \textstyle\sum F_{NOISE} &\equiv \text{disturbance forces} \end{aligned}$$

$\vec{F}_{NOISE}$ can be depicted with the wave equation, since we are trying to show the small disturbances propagating in the pool. However, we are given that the competition takes place in stationary pools and only one vehicle will be in the pool at one time. The vehicle is to be placed in the center of the pool, thus the walls would not generate enough forces to affect the vehicle either. Though there will also be divers ensuring the safety of the pilot underwater, we assume that there will be

the same number of divers on each side of the vehicle at all times, and the divers wouldn't create enough disturbance on the vehicle to begin with.

By focusing solely in the roll channel, we can then simplify the equations of motion down to purely the roll plane, which simplifies from six degrees of freedom down to four degrees of freedom.

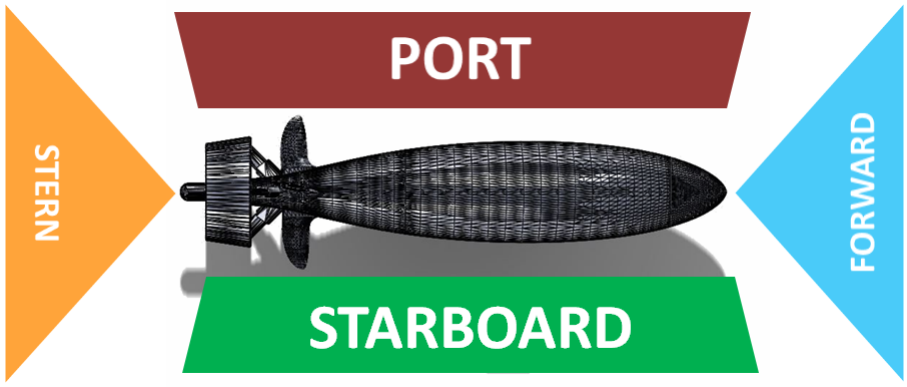

Figure 3.2: Nautical terms of a watercraft

Translation Equations

$$\dot{x} = cos(\psi)cos(\theta)u + [-sin(\psi)cos(\psi) + cos(\psi)sin(\phi)sin(\theta)]v + [sin(\psi)sin(\phi) + cos(\psi)sin(\theta)]w \quad (3.43)$$

$$\phi = p + sin(\phi)tan(\theta)q + cos(\phi)tan(\theta)r \quad (3.44)$$

Controller Equation

$$|\delta_{ep}| = |\delta_{es}| = \begin{cases} \delta_{ep} \\ \delta_{es} \end{cases} \quad (3.45)$$

Even though there are two rudders and two elevators, we will only be controlling the two elevators of the four control surfaces. Furthermore, we can separate the two elevators into the nautical terms of orientation (Fig.3.2), port and starboard, but we

will be controlling them as opposing forces of the same magnitude. Therefore, we can assume that our controllers will be somewhat coupled (Eq.3.45).

3.10 Summation of Forces in the Roll-Axis

To form the summation of forces in the roll-axis, We can assume that our plant model controls the stability, added mass, and dampening. The propulsion torque will be considered in the disturbance in relation to speed ($\alpha\mathbf{u}$). And the controller, in addition to accounting for the propulsion torque, will also consider the roll lift. We can also neglect the surge and roll modes, assuming ϕ to be constant and $p_o = \phi_o = 0$. Therefore, we can get the summation of forces (Eq.3.46) and the equations of motion (Eq.3.48) in the roll-axis.

$$\sum M_L = \underbrace{(y_g W - y_B B)cos(\theta)cos(\phi) - (z_g W - Z_B)cos(\theta)sin(\theta)}_{\text{stability}} + \underbrace{K_{p|p|}p|p| + K_{\dot{p}\dot{p}}}_{\text{added mass and dampening}} + \underbrace{K_{PROP}}_{\text{propulsion torque}} + \underbrace{f(\delta_{ep}, \delta_{es}, \nu, t)}_{\text{roll lift}} \quad (3.46)$$

The roll lift is a function of the elevator angles, the speed, and time component. Note that the speed is not controllable since it will be at the the pilot's discretion, but it is observable, so it is set at a constant value.

3.11 Equation of Motion in the Roll-Axis

$$\sum L = \underbrace{I_{xx}\dot{p}}_{\spadesuit} + \underbrace{(I_{zz} + I_{yy})qr}_{\diamondsuit} - m\,\underbrace{z_g(v - wp + ur)}_{\clubsuit} \quad (3.47)$$

We first derive the EoM in the roll-axis and split it up into three subsections. The first section ($\spadesuit$) is the moment of inertia about x times the roll rate of change. The second section ($\diamondsuit$) is the moment of inertia about y and z multiplied by the pitch and yaw rates, however, since we yaw during roll, but not pitch, we can set $q = 0$, therefore, the entire second part of the equation goes away. The last section of the

equation (♣) is multiplied by mass m, which is irrelative to the center of gravity and thus taken out of the section, but the rest depicts the lean caused by the displacement of the center of gravity. Specific to the roll-axis, we can neglect sway and heave, $v = 0$ and $w = 0$, therefore, we only keep the last part of the parenthesis, where ur is the lean and an important factor for roll control. After taking out everything we are neglecting, we arrive at the following equation:

$$\therefore \sum L = I_{xx}\dot{p} - mz_G ur \tag{3.48}$$

3.12 Roll, Pitch, and Yaw Motions with Gravity Vector

Roll ϕ

$$\phi = \begin{bmatrix} 1 & 0 & 0 \\ 0 & cos(\phi) & sin(\phi) \\ 0 & -sin(\phi) & cos(\phi) \end{bmatrix} \tag{3.49}$$

$$\bar{g}_\phi = \begin{bmatrix} 0 \\ gsin(\phi) \\ gcos(\phi) \end{bmatrix} \tag{3.50}$$

Pitch θ

$$\theta = \begin{bmatrix} cos(\theta) & 0 & -sin(\theta) \\ 0 & 1 & 0 \\ sin(\theta) & 0 & cos(\theta) \end{bmatrix} \tag{3.51}$$

$$\bar{g}_\theta = \begin{bmatrix} -gsin(\theta) \\ 0 \\ gcos(\theta) \end{bmatrix} \tag{3.52}$$

Yaw ψ

$$\psi = \begin{bmatrix} cos(\psi) & sin(\psi) & 0 \\ -sin(\psi) & cos(\psi) & 0 \\ 0 & 0 & 1 \end{bmatrix} \tag{3.53}$$

$$\bar{g}_{\psi} = \begin{bmatrix} 0 \\ 0 \\ g \end{bmatrix} \tag{3.54}$$

By using the roll, pitch, and yaw motions with the gravity vector and assuming z' is vertical down, we get the following composite transformation:

$$\bar{x} = \phi \bar{x}' \tag{3.55}$$

$$\bar{x} = \theta \bar{x}' \tag{3.56}$$

$$\bar{x} = \psi \bar{x}' \tag{3.57}$$

where

$$\bar{x} \equiv \text{sub-frame}$$

$$\bar{x}' \equiv \text{rotated axes}$$

$$\bar{x} = \begin{bmatrix} 1 & \psi & -\theta \\ -\psi & 1 & \phi \\ \theta & -\phi & 1 \end{bmatrix} \bar{x}' \tag{3.58}$$

$$\bar{g} = \begin{bmatrix} -\theta \\ \phi \\ 1 \end{bmatrix} g \tag{3.59}$$

3.13 Roll Dynamics

Since the vehicle is set to travel in a straight trajectory, we can assume the changes of the attitude (in Euler angles) are small, therefore, the hydrostatic moments acting on the submarine about center of buoyancy will be the following:

$$K_{HS} = -y_G W - z_G W \phi \tag{3.60}$$

$$M_{HS} = -z_G W\theta - x_G W \tag{3.61}$$

$$N_{HS} = -y_G W\phi - z_G W\theta \tag{3.62}$$

Thus, the roll dynamics will result as:

$$\frac{\phi(s)}{\delta_e(s)} = \frac{\frac{4K_{uu\delta_e}}{z_g W}}{(\frac{I_{xx}-K_{\dot{p}}}{z_g W})s^2 + 1} \tag{3.63}$$

where

$\phi \equiv$ roll

$\delta_e \equiv$ elevator angle

$K_{uu\delta_e} \equiv$ elevator effectiveness

$K_{\dot{p}} \equiv$ added mass

$z_g \equiv$ coordinates of the CG in z-axis relative to CB

Furthermore, roll dynamics are insensitive to speed and exhibits marginally stable poles [4], thus, we can ignore negligibly small quantities, so $\dot{\phi} = p, \dot{\theta} = q,$ and$\dot{\psi} = r$. We can also use the following matrices to define the mapping between the linear and angular velocities and the position and orientation.

$$\vec{w}_b = p\hat{x}_b + q\hat{y}_b + r\hat{z}_b \tag{3.64}$$

$$\boldsymbol{\omega} = \dot{\phi} + \dot{\theta} + \dot{\psi} \tag{3.65}$$

$$= p + q + r \tag{3.66}$$

$$\begin{Bmatrix} p \\ q \\ r \end{Bmatrix} \triangleq R_1(\phi)R_2(\theta)R_3(\psi) \begin{Bmatrix} 0 \\ 0 \\ \dot{\psi} \end{Bmatrix} + R_1(\phi) \begin{Bmatrix} 0 \\ \dot{\theta} \\ 0 \end{Bmatrix} + \begin{Bmatrix} \dot{\phi} \\ 0 \\ 0 \end{Bmatrix} \tag{3.67}$$

$$= \begin{bmatrix} 0 & 0 & 0 \\ 0 & cos(\phi) & sin(\phi) \\ 0 & -sin(\phi) & cos(\theta) \end{bmatrix} \begin{Bmatrix} -sin(\theta)\dot{\psi} \\ 0 \\ cos(\theta)\dot{\psi} \end{Bmatrix} + \begin{bmatrix} 0 \\ cos(\psi)\dot{\theta} \\ sin(\psi)\dot{\theta} \end{bmatrix} + \begin{bmatrix} \dot{\psi} \\ 0 \\ 0 \end{bmatrix} \tag{3.68}$$

$$= \begin{bmatrix} -\dot{\psi}sin(\theta) + \dot{\phi} \\ \dot{\psi}cos(\theta)sin(\psi) + cos(\psi) + \dot{\theta} \\ \dot{\psi}cos(\phi)cos(\theta) - \dot{\theta}sin(\psi) \end{bmatrix} \tag{3.69}$$

$$= \begin{bmatrix} 1 & 0 & -sin(\theta) \\ 0 & cos(\psi) & cos(\theta)sin(\psi) \\ 0 & -sin(\psi) & cos(\psi)cos(\theta) \end{bmatrix} \begin{Bmatrix} \dot{\phi} \\ \dot{\theta} \\ \dot{\psi} \end{Bmatrix} \tag{3.70}$$

And in reverse,

$$\begin{Bmatrix} \dot{\phi} \\ \dot{\theta} \\ \dot{\psi} \end{Bmatrix} = \begin{bmatrix} p + [qsin(\phi) + rcos(\phi)tan(\theta)] \\ qcos(\phi) - rsin(\phi) \\ [qsin(\psi) + rcos(\phi)]\frac{1}{cos(\theta)} \end{bmatrix} \tag{3.71}$$

$$= \begin{bmatrix} p + [qsin(\phi) + rcos(\phi)tan(\theta)] \\ qcos(\phi) - rsin(\phi) \\ [qsin(\psi) + rcos(\phi)]\sin(\theta) \end{bmatrix} \tag{3.72}$$

$$= \begin{bmatrix} 1 & sin(\phi)tan(\theta) & cos(\phi)tan(\theta) \\ 0 & cos(\phi)cos(\phi) & -sin(\phi) \\ 0 & sin(\phi)sec(\theta) & cos(\phi)sec(\theta) \end{bmatrix} \begin{Bmatrix} p \\ q \\ r \end{Bmatrix} \tag{3.73}$$

3.14 Added Mass

When the watercraft is accelerating or decelerating in the water, we have to consider additional hydrodynamic forces acting on the hull. Quantities of fluid moving around

the hull can be determined using the theoretical method [5] and for our purposes, we can assume the vehicle to reside in inviscid fluid (e.g. air and water), i.e. water fluid density at $1000kg/m^3$.

3.14.1 Added Mass of the Hull

The inertia moment of the displaced water is approximately the moment of inertia of teh equivalent ellipsoid that is our hull. However, since the human-powered submarine will be encased in water when it is moving, we can exclude the inertia moment of the displaced water. Based on the descriptions of the human-powered submarine found in Section 2.1.1, we assume *The Underdawg* as a slender body, whose characteristic length in the longitudinal x-direction is considerably larger than in the y- and z-directions and small lateral variations [6]. Since we can assume rotational symmetry in the x-axis, the added mass matrix of the HPS hull can be written as

$$M_{a,hull} = \begin{bmatrix} m_{11} & 0 & 0 & 0 & 0 & 0 \\ 0 & m_{22} & 0 & 0 & 0 & m_{26} \\ 0 & 0 & m_{33} & 0 & m_{35} & 0 \\ 0 & 0 & 0 & 0 & 0 & 0 \\ 0 & 0 & m_{53} & 0 & m_{55} & 0 \\ 0 & m_{62} & 0 & 0 & 0 & m_{66} \end{bmatrix} \tag{3.74}$$

Since the HPS has rotational symmetry and is in inviscid fluid (i.e. water), we can use the potential flow theory, and further simplify the matrix, where

$$\begin{aligned} m_{22} &= m_{33} \\ m_{26} &= m_{62} \\ m_{35} &= m_{53} \\ m_{55} &= m_{66} \end{aligned} \tag{3.75}$$

$$
\begin{aligned}
m_{11,hull} &= -k_1 \frac{4}{3} \pi \rho r_1 r_2^2 \\
m_{22,hull} &= \int_L \pi \rho r_{hull}^2 dx \\
m_{26,hull} &= \int_L \pi \rho x r_{hull}^2 dx \\
m_{33,hull} &\equiv m_{22,hull} = \int_L \pi \rho r_{hull}^2 dx \\
m_{35,hull} &= -\int_L \pi \rho x r_{hull}^2 dx \\
m_{44,hull} &= 0 \\
m_{53,hull} &= m_{35,hull} = -\int_L \pi \rho x r_{hull}^2 dx \\
m_{55,hull} &= \int_L \pi \rho x^2 r_{hull}^2 dx \\
m_{62,hull} &= m_{26,hull} = \int_L \pi \rho x r_{hull}^2 dx \\
m_{66,hull} &\equiv m_{55,hull} = \int_L \pi \rho x^2 r_{hull}^2 dx
\end{aligned}
\tag{3.76}
$$

Where

$L \equiv$ longitudinal length of the hull

$r_1 \equiv$ longitudinal radius of the hull

$r_2 \equiv$ radius of the hull

$r_{hull} \equiv$ hull radius over vehicle length

$k_1 \equiv$ one of the Lambs k-factors

$\varrho \equiv$ constant describing the relative proportions of the hull

$$
r_{hull} = \frac{r_2}{r_1} \tag{3.77}
$$

$$k_1 = \frac{\varrho}{2 - \varrho} \tag{3.78}$$

$$\varrho = \frac{2(1-e^2)}{e^2}\left[\frac{1}{2}ln\Big(\frac{1+e}{1-e}\Big) - e\right] \tag{3.79}$$

$$e = 1 - \frac{r_2^2}{r_1} \tag{3.80}$$

From the HPS parameters given in Section 2.1.1, we know $r_1 = 1m$ and $r_2 = 0.37129m$. We can then calculate the following values using Equations 3.77 to 3.80.

Table 3.2: Hull Added Mass Initial Calculations

Variable	Value	Unit
r_1	1.00000	m
r_2	0.37129	m
r_{hull}	0.37129	-
e	0.86214	-
ϱ	0.30357	-
k_1	0.17895	-

From Table 3.3, the hull added mass matrix (Eq.3.74) can be written as

$$M_{a,HPS,hull} = \begin{bmatrix} 3.150 & 0 & 0 & 0 & 0 & 0 \\ 0 & 2332.900 & 0 & 0 & 0 & 866.177 \\ 0 & 0 & 2332.900 & 0 & -866.177 & 0 \\ 0 & 0 & 0 & 0 & 0 & 0 \\ 0 & 0 & -866.177 & 0 & 3110.500 & 0 \\ 0 & 866.177 & 0 & 0 & 0 & 3110.500 \end{bmatrix} \tag{3.81}$$

Table 3.3: Hull Added Mass Coefficients

Coefficient	Values
$m_{11,hull}$	3.150
$m_{22,hull}$	2332.900
$m_{26,hull}$	866.177
$m_{33,hull}$	2332.900
$m_{35,hull}$	-866.177
$m_{44,hull}$	0
$m_{53,hull}$	866.177
$m_{55,hull}$	3110.500
$m_{62,hull}$	866.177
$m_{66,hull}$	3110.500

3.14.2 Added Mass of the Rudders

Next, we want to calculate the added mass of the rudders, which is derived as

$$M_{a,rudder} = \begin{bmatrix} m_{11} & 0 & 0 & 0 & 0 & 0 \\ 0 & m_{22} & 0 & 0 & 0 & 0 \\ 0 & 0 & m_{33} & 0 & 0 & 0 \\ 0 & 0 & 0 & m_{44} & 0 & 0 \\ 0 & 0 & 0 & 0 & m_{55} & 0 \\ 0 & 0 & 0 & 0 & 0 & m_{66} \end{bmatrix} \tag{3.82}$$

Here, m_{44} and m_{55} are the rotational added mass. m_{44} is the added inertia rotated about the x-axis, with origin at the center of the rudder. m_{55} is the added inertia due to a pitching moment rotated about the y-axis [6].

$$
\begin{aligned}
m_{11,rudder} &= k_{trans}\frac{\pi\rho t^2 b^3}{4} \\
m_{22,rudder} &= k_{trans}\frac{\pi\rho t^2 c^3}{4} \\
m_{33,rudder} &= k_{trans}\frac{\pi\rho c^2 b^3}{4} \\
m_{44,rudder} &= k_{rot}\frac{\pi\rho b^3 c^2}{48} + CB^2_{rudder,y} m_{33,rudder} \\
m_{55,rudder} &= k_{rot}\frac{\pi\rho b^2 c^3}{48} + CB^2_{rudder,x} m_{33,rudder} \\
m_{66,rudder} &= 0
\end{aligned}
\tag{3.83}
$$

Where

$$
\begin{aligned}
c &= \text{chord of the control surface } [m] \\
b &= \text{span of the control surface } [m] \\
t &= \text{thickness of the control surface } [m] \\
S &= \text{planform area or the surface area of the rudder} \\
AR &= \text{aspect ratio} \\
k_{trans} &= \text{added inertia in translation} \\
k_{rot} &= \text{added inertia in rotation} \\
CB_{rudder,x} &= \text{center of buoyancy of the rudder in the x-direction} \\
CB_{rudder,y} &= \text{center of buoyancy of the rudder in the y-direction}
\end{aligned}
$$

$$
AR = \frac{b^2}{S} \tag{3.84}
$$

$$
k_{trans} = \frac{1}{\sqrt{1 + \frac{1}{AR}}} \tag{3.85}
$$

$$
k_{rot} = \frac{1}{AR} \tag{3.86}
$$

Next, we know the control surfaces, i.e. the rudders, uses the NACA 0008 Airfoil (naca0008-il) profile, and using the dimensions from Fig.2.5, we can calculate the added mass of the rudders and the initial calculations using Eq.3.84 to 3.86.

Table 3.4: Rudder Added Mass Initial Calculations

Variable	Value	Unit
c_{rudder}	0.247	m
b_{rudder}	0.5	m
t_{rudder}	0.01977	m

Table 3.5: Rudder Added Mass Coefficients

Coefficient	Values
$m_{11,rudder}$	0.0324
$m_{22,rudder}$	0.0039
$m_{33,rudder}$	5.0621
$m_{44,rudder}$	0.0986
$m_{55,rudder}$	-0.0026
$m_{66,rudder}$	0

From Table 3.5, the hull added mass matrix (Eq.3.82) can be written as

$$M_{a,HPS,rudder} = \begin{bmatrix} 0.0324 & 0 & 0 & 0 & 0 & 0 \\ 0 & 0.0039 & 0 & 0 & 0 & 0 \\ 0 & 0 & 5.0621 & 0 & 0 & 0 \\ 0 & 0 & 0 & 0.0986 & 0 & 0 \\ 0 & 0 & 0 & 0 & -0.0026 & 0 \\ 0 & 0 & 0 & 0 & 0 & 0 \end{bmatrix} \tag{3.87}$$

Chapter 4
TECHNICAL DISCUSSION

This chapter details the significant test campaign that was performed to validate the system as well as the simulation results. The initial half of the tests conducted involved a lot of calibration and coding of the electronics system and the latter portion are geared towards theoretical simulations through MATLAB and Simulink.

4.1 Arduino Test

As mentioned in the hardware section, the microcontroller used for this system is the Arduino Nano 33 IoT. There were three of the same microcontroller purchased and tested to ensure that the hardware wouldn't be a source of error. An LED check, sensor output, and orientation test was conducted, and one of the Arduino was found to not be in working condition, but two would be able to move forward to the next part.

4.1.1 Initial Microcontroller Tests

After validating the hardware to be in proper working condition, three Arduino codes were developed to allow communication between the computer and the microcontroller. Creating these codes provided options for users to choose connectivity via serial port, WiFi, or Bluetooth. A serial port connection was easiest when working with the microcontroller alone, testing and uploading codes while it sat on the desk. The WiFi connection was intended for ground testing inside the building and the Bluetooth code is the final intent for underwater purposes and connectivity between the computer and microcontroller outside. To further define the codes, it was impor-

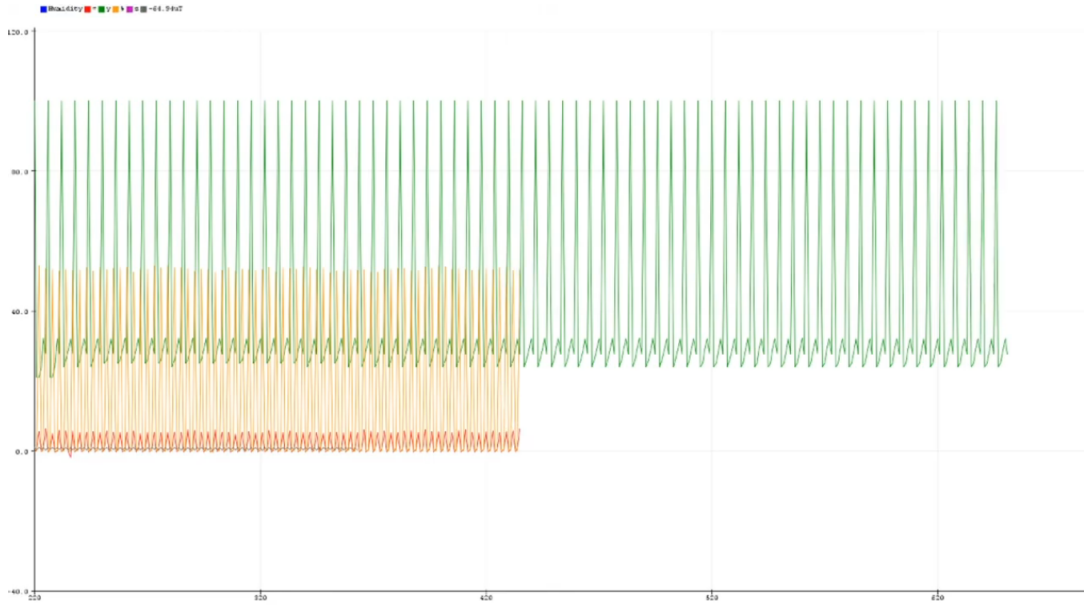

Figure 4.1: Arduino Prior to Calibration

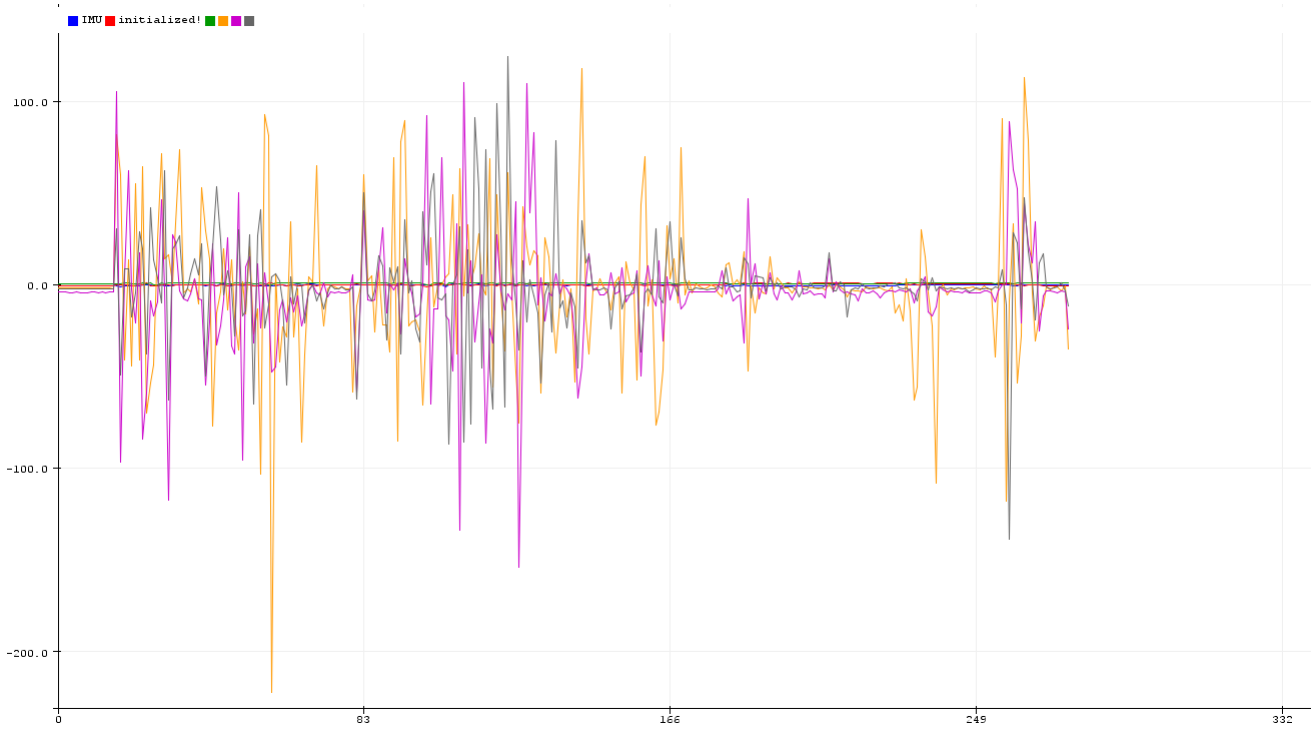

Figure 4.2: Arduino Calibrated

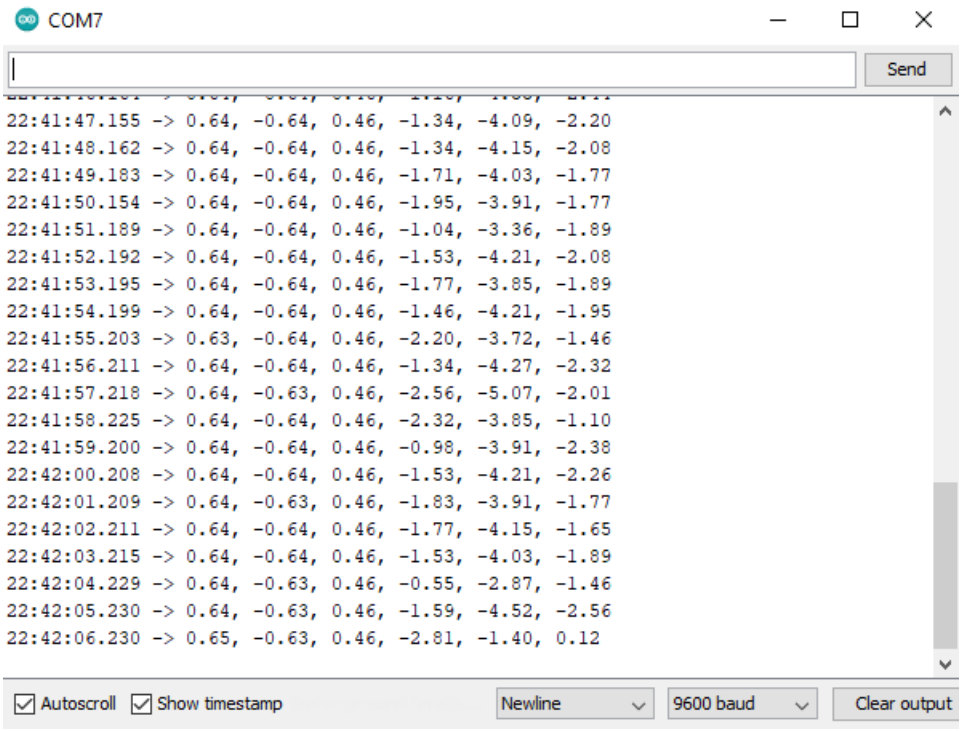

Figure 4.3: Initial Arduino Sensor Output

tant to calibrate the sensor outputs into a proper form corresponding to one another. Prior to calibration (see Fig.4.1), the microcontroller was defaulted at a baud rate of 9600 bps, but outputs the rest of the information at different speeds. Each output had to be recalculated so they would all produce an output at the same time, as shown in Fig.4.2.

4.1.2 Arduino to MATLAB

Since the calculations and PID controller will be developed and used via MATLAB Simulink, we had to first output data from Arduino to MATLAB. However, this requires a change in format from Arduino to MATLAB. We first need to change the microcontroller output into a string used to create the Arduino object in MATLAB. The data produced by the accelerometer and gyrometer had to be integrated to MATLAB with a simple conversion based on the specification angle devised by the manufacturer and divided by the total angle. The string data outputted by the accelerometer and gyrometer was multiplied by 2/32768 and 250/32768, respectively, to produce the same values as it did via the Arduino IDE. The code created allows the linear values to be read from all direction, x, y, and z, and is calculated based on the sensor orientation.

4.1.3 MATLAB to Arduino

After the values are analyzed through MATLAB and a change in control is determined from Simulink, the MATLAB data then outputs its command to the Arduino. Without the human-powered submarine nor physicals fins to command, the Arduino command is not able to fully validate the research. Instead, we can further analyze the data through MATLAB and Simulink as shown below.

4.2 Pilot Input

Since we are unable to see the results of the project through actual vehicle implementation, we can simulate the results. To mock pilot input during the experimental stage, a Logitech F310 Gamepad, fitted with Simulink controls demonstrates the overall movement of the mocked vehicle. This requires installing the Pilot Joystick block

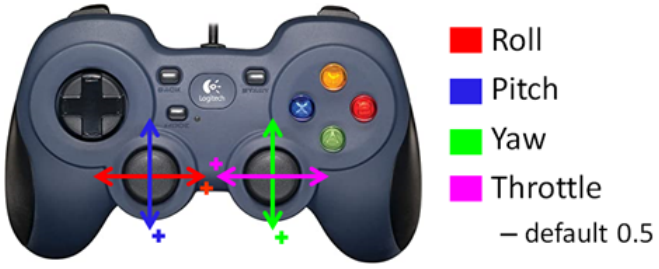

Figure 4.4: Pilot Input via Logitech F310 Gamepad

from the Aerospace Toolbox, which allows the left joystick on the on the controller to simulate roll and pitch and right joystick to simulate yaw and throttle, with the throttle defaulted at 0.5 (with -1 or +1 as the farthese values in both directions).

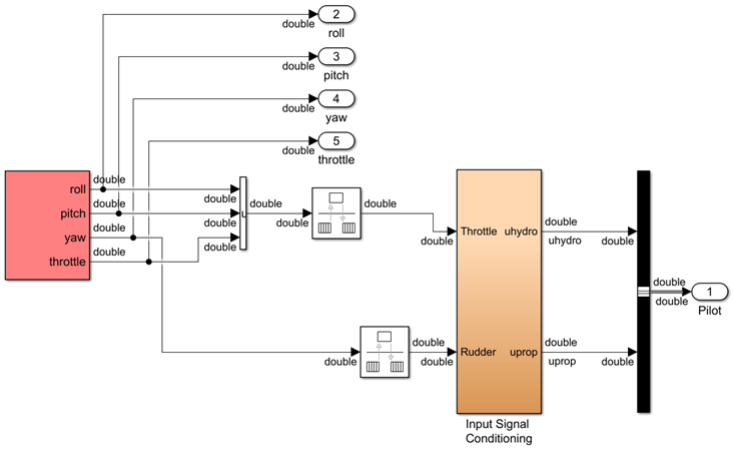

Figure 4.5: Pilot Input via Simulink

4.3 Route Tracking Analysis

To demonstrate the feasibility of the sensor in reliable data for accurate location tracking in a short distance, the sensor was placed inside a mock surrogate to simulate the electronics inside the HPS and taken for a short round trip drive at a constant 25 mph.

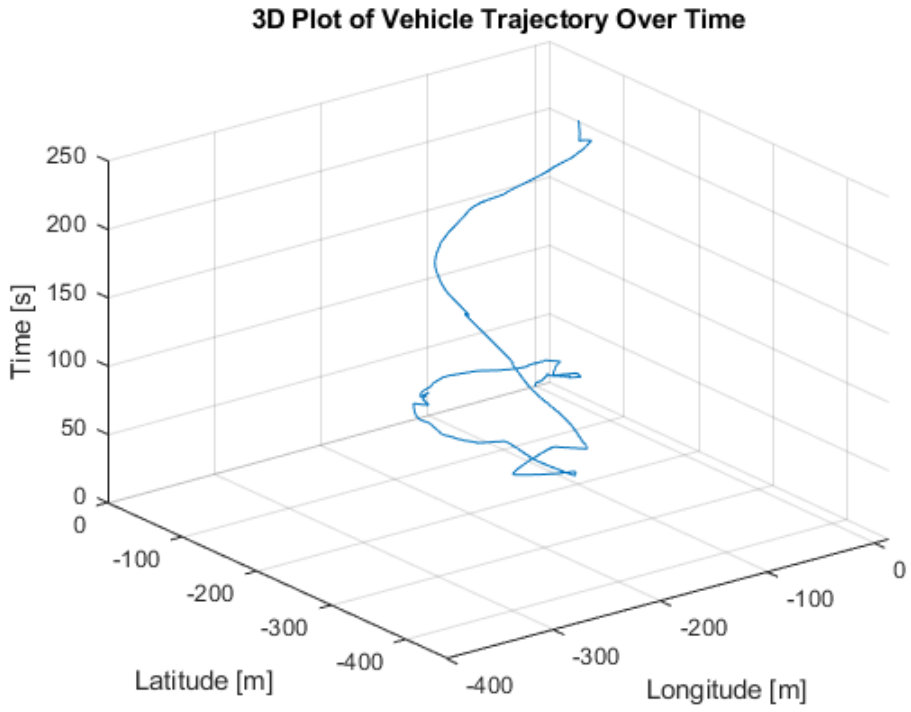

Figure 4.6: Vehicle Trajectory Over Time

Above and below are data generated on two different plots, one to show the overall trajectory over time (Fig.4.6), while the latter shows the latitudinal and longitudinal changes (Fig.4.7) during the test. Based on the settings defined to be attuned to the rest of the electronics onboard the human-powered submarine, the sensor is parameterized to take in one set of data every $1000ms$ or $1s$.

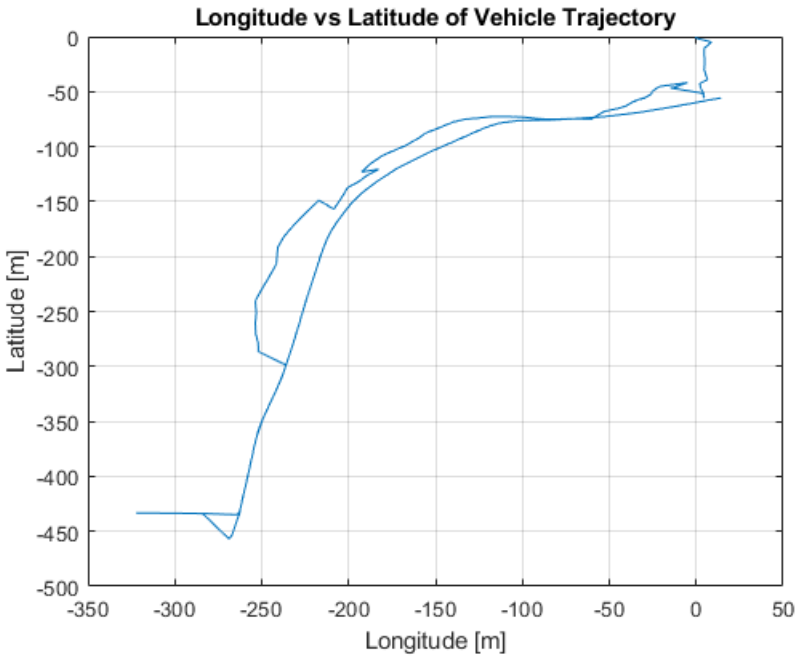

Figure 4.7: Longitude vs Latitude of Vehicle Trajectory

4.4 Control Loop Analysis

A Proportional Integral Derivative (PID) controller is designed for horizontal stability and its gain values is set to inherit the form:

$$PID(s) = K_p + \frac{K_i}{s} + K_d s \tag{4.1}$$

It uses a control feedback loop that monitors where the output should be by keeping the controlled parameter constant. This loop continuously takes information on what it is currently set at and determines the changes it needs to make before sending controls to the actuators on the system. The $r(t)$ is the setpoint or reference point, setting a specific desired process value. Adding the sensor measurements and accounting for errors, it then goes to the PID controller. The PID controller allows gain adjustments by tuning constants to apply control to the desired output. The desired output is then pushed through to the parameter we want to control, adding

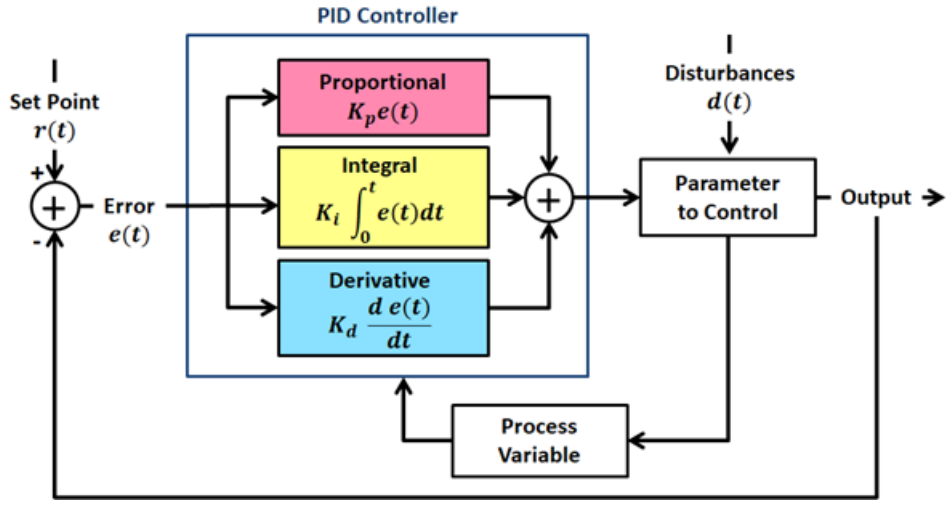

Figure 4.8: Typical PID Control Loop

disturbances or noises that may affect the system. The entire process then cycles around and the loop is repeated.

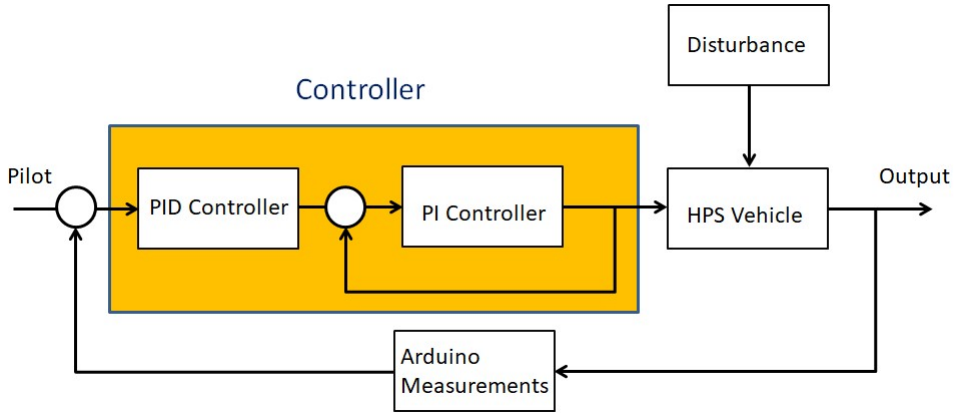

Figure 4.9: Simplified PID Control Loop

For this research, an initial reference point along with the manual pilot control and automatic and continuous sensor outputs represents $r(t)$. We implement a cascade control system with both a PID and PID controller (Fig.4.9), where the outer loop stabilizes the roll factor, and the inner loop is a back-up controller in the case the

outer loop is unable to fully stabilize. The parameter we want to control is the human-powered submarine and since we assume the vehicle is inside a pool the possible disturbance $d(t)$ is just small variable noise. The system output becomes the actual roll of the vehicle while a desired roll is continuously cycled throughout the loop as the measured output.

For the PID controller, the initial PID gain values is set at $K_p = 4$, $K_i = 1$, and $K_d = 1$. Though the elevators, starboard and port, are both projected in the full control loop diagram (Fig.4.10), they are coupled, which results in its responses to project equal magnitude in opposing signs.

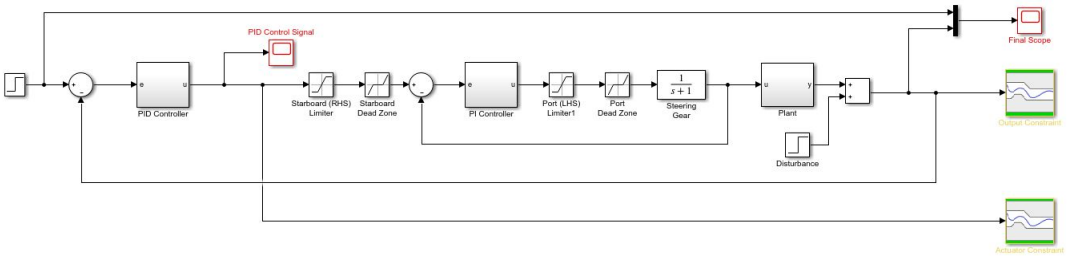

Figure 4.10: PID Control Loop in Detail

When simulated with a pilot pitch/roll command and constant thrust of $\mathbf{v} = 0.5m/s$, we see from the outer control loop bode plot (Fig.4.11) that the magnitude increases, but return back to the trim value at zero within a second. Furthermore, since the control loop is solely designed for horizontal stability, the human-powered submarine will have small steady states, which are relatively small and therefore negligible.

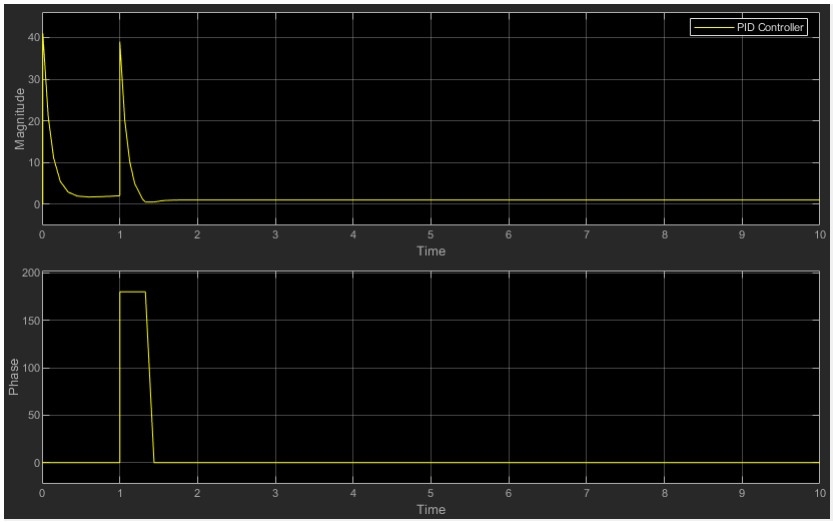

Figure 4.11: Bode Plot of PID Controller

As mentioned earlier, the second controller is used as a back-up in the case the first controller fails. In the case there was an error for which the first controller was unable to account for, the graph for the second controller should remain at zero. From the bode plot of the inner control loop shown in Fig.4.12, we can see that both outputs remained at zero, which means we can substantiate the data produced by the first controller.

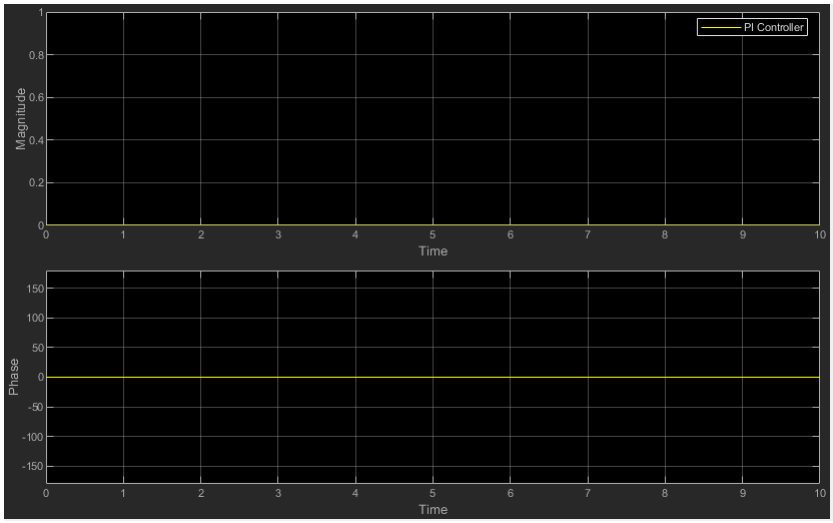

Figure 4.12: Bode Plot of PI Controller

4.5 Constraint Analysis

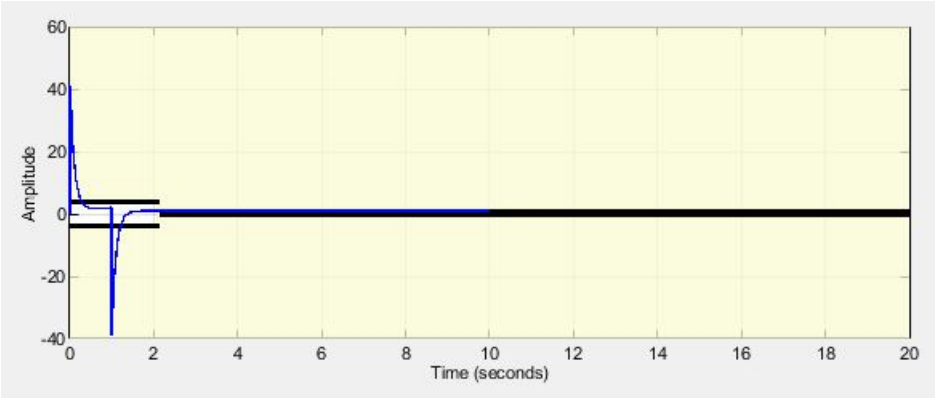

Figure 4.13: Actuator Constraint

The human-powered submarine requires near horizontal stability, but to implement it on an underwater vehicle and assume the requirement would hold is unrealistic. It is nearly impossible to always assume the vehicle will always be at a perfect zero degrees, and if the system is set to try to stabilize every time it is not, it will

be putting in much more effort than it is needed. Therefore, two constraint blocks are added to the model, to define a set of parameters and an expression to constrain those parameters.

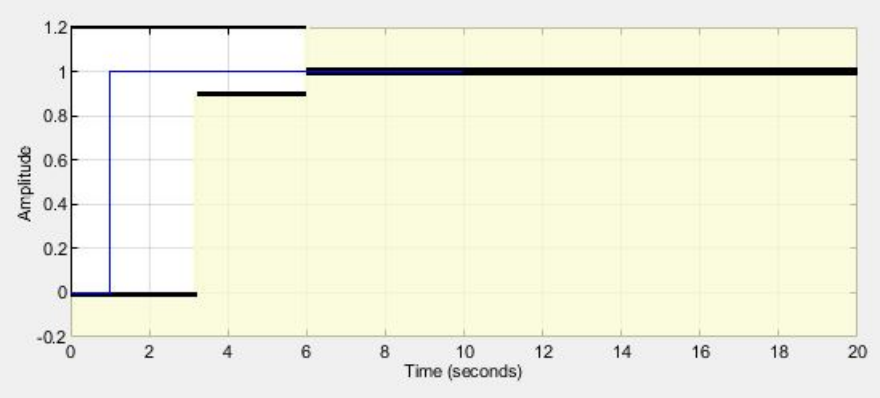

Figure 4.14: Output Constraint

The actuator constraint (Fig.4.13) sets the amplitude to stabilize if and only if it is more than 0 deg $\pm$2 deg. The output constraint (Fig.4.14) sets the fin deflections to be no more than 45 deg, which is the furthest is it allowed without damaging the integrity of the control surfaces. And since the control surfaces are coupled, only one of the output graph is shown.

4.6 PID Controller vs Control Surfaces

Figure.4.15a combines the vehicle stability along the horizon and the elevators acting on the system. In yellow depicts where the initial signal was received and stabilized to zero. While blue depicts the fin deflection angle made to stabilize the vehicle. Though the latter is harder to see, a zoomed in version (Fig.4.15b) is shown, and we can see that there was a small change in blue.

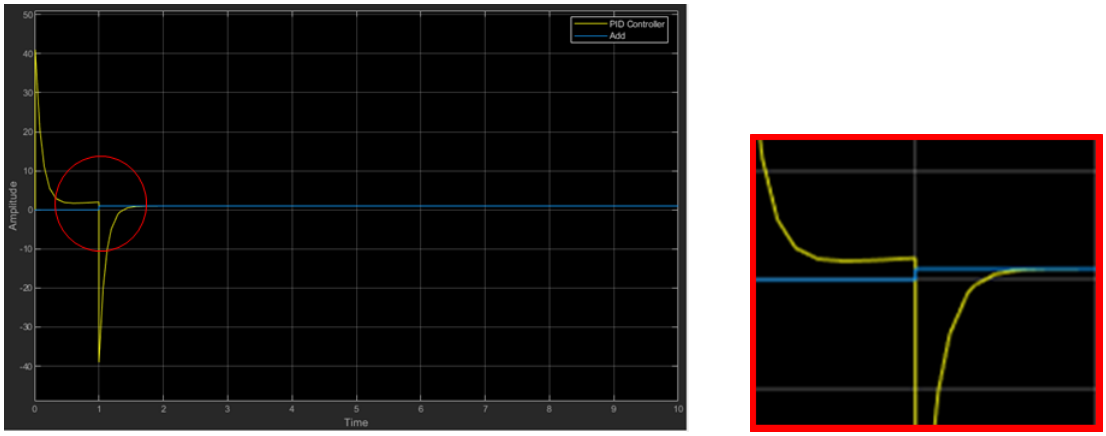

(a) Overall (b) Zoomed In

Figure 4.15: Vehicle Horizontal Stability vs Control Surface Fin Deflection

Chapter 5

FINAL REMARKS

Inspired by the challenges entailed in a human-powered submarine, we were able to successfully conduct the objectives identified. Enhancing the underwater vehicle by changing its manual maneuverability from 3D to 2D reduces the pilot's work, fuel consumption, and time trajectory. Further research into the application can eventually be integrated onto larger vehicles, enabling stability in underwater vehicles with multiple onboarding personnel. The demand in simplification for technological advancement will continue to increase, whether through expanding current capabilities or discovering new methods for better application usage.

5.1 Work Summary

This thesis successfully addressed three primary areas of interest: sensor route tracking, using cascade control architecture to design PID control loops for horizontal stability, and implementation on simulated hardware applications. By simulating the experiment with a manual controller and microcontroller, the information produced to the computer is then analyzed and outputted into better visual representation and calculated for automatic maneuverability. The measurements used for this simulation were simplified based on the mathematical interpretations from Chapter 3. We assumed a stationary pool with no any substantial noise to add in addition to the random noise. We also assume for the controller to begin under water, i.e. the calculations do not fully encompass all water conditions. Water conditions varied would include the density and the unpredictability of the body of water (e.g. river or ocean waters).

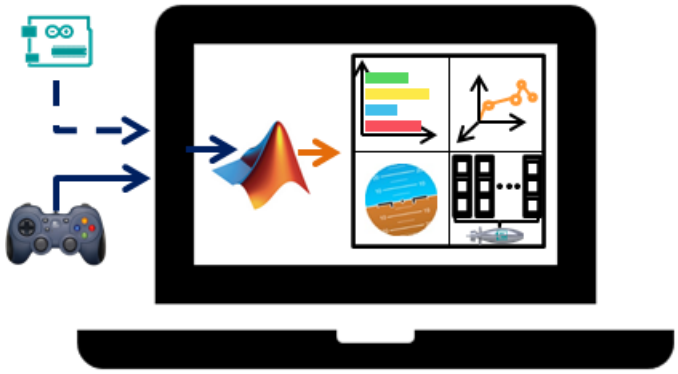

Figure 5.1: Visualization of the Autonomous Roll Control

From the visual representation to the PID controller that was created, the project demonstrated the application's feasibility as a roll control method. The vehicle trajectory information provided a visual representation of position and orientation tracking. While the PID controller constructed via Simulink produced an autonomous control for horizontal stability and validates the actuators being controlled during simulation. By testing the theoretical side of this project with physical hardware integration and output visualization, we demonstrated and simulated hardware implementation, which further legitimizes this project and emphasizes its practicability.

5.2 Future Work

Many of the work described below requires multiple personnel in a small vicinity, thus was not tested for the duration of this thesis. However, this project provided valuable insight and demonstrated the feasibility integrating this system into actual hardware. We can further expand this research into a bigger picture, as shown in

Fig.5.2. This project extended from creating the electronic system, integrating the system into a configurable watertight container, to being able to integrate it into a human-powered submarine. After further testing, it can then be integrated into larger unmanned (or manned) underwater vehicles for deep water exploration. There are a lot more research we can expand into as a continuation of this thesis. The future work suggested are recommended to be tested in similar order, but some may not be a prerequisite to the rest.

Figure 5.2: The bigger picture from this project

5.2.1 Surrogate UUV Underwater Test

Before putting the entire system underwater, we want to ensure that the commercially customized fuselage is capable of keeping water out of the the interior. Depending on how specific we want the information to be, there are many ways to do this. To demonstrate if any leaks are detected, this can be as simple as padding paper towels inside and checking to see if they are wet. For more detailed information, we can

also place leak sensor probe tips to the openings of the fuselage and use a water leak sensor to detect water leaking into the watertight enclosure.

After checking if the enclosure is properly sealed, we also want to test the enclosure at various depths. The user manual guarantees depths of $100m$, therefore, we can slowly dive further into the water with the enclosure. This would be more geared towards submarines in the open water. For the purpose of the human-powered submarine, the enclosure would only need to be tested down to a depth of $7m$, since the longest pool used for competition is roughly $575m$ long and $6.7m$ deep [7].

5.2.2 RC Vehicle Ground Testing

While we have demonstrated the Arduino's position tracking capabilities with a round trip car ride, we also want to test the limits on the minimum amount of change needed for it to be tracked. The mounting process can be as simple as securing the Arduino down on an RC vehicle with a zip tie. However, detailed tests would include keeping the vehicle at constant velocity with a small range of error, and experimenting with variable maneuvers mimicking the human-powered submarine. Some of this would include traveling in a straight trajectory, performing really wide turns, etc.

5.2.3 Surrogate UUV Assembly

The intended purpose for the interior components is to be easily accessible and interchangeable. It is highly recommended to 3D print a skeleton for the enclosure with tight fit settings accommodating the form factors of each interior component. Depending on the material, 3D printed parts are more customization and lighter in mass, thus decreasing the amount of space needed but still keeping the components secured. The assembly would include the watertight enclosure as the fuselage, the 3D printed skeleton tightly fitted into the interior, and accommodate space for the Arduino, batteries to power the Arduino, and wires, all of which will keep the center of gravity and center of buoyancy at the recommended location (scaled to the HPS).

5.2.4 Surrogate UUV Assembly with Control Surfaces

The current assembly set-up for the surrogate UUV is an independent system that outputs position and adjusts the local horizontal attitude based on the input references provided by the pilot, vehicle, and sensor outputs. This set-up relies on a vehicle for testing. However, we can set it up as a scaled miniature version of a submarine, following submarine dynamics, and add control hardware to the exterior. Adding control surfaces such as the rudder controls and a propulsion system would turn the independent system into a UAV so further testing can be conducted with just the surrogate UUV as a standalone alone system.

5.2.5 Surrogate UUV Ground Test

After deducing the Arduino sensors' capabilities, it would be wise to conduct a ground test with all of the electronic components inside the surrogate UUV prior to another test under water. To do so, all components on the electronic bay needs to be safely secured. The surrogate UUV will then be placed on an unmanned ground vehicle and calibrated prior to the start of its run. In doing so, we can further validate the tracking accuracy by comparing its data with the previous test conducted while taking the electronics in a car.

5.2.6 Surrogate UUV Underwater Test

With all the electronic components fastened and properly sealed inside the surrogate UUV, the fully enclosed system can be tested under water. It is important to test the range and accuracy of the connectivity while the system is under water so we can ensure we don't lose connection between the surrogate UUV and the computer controlling it.

5.2.7 Interchangeable Components

Furthermore, we can make the components more easily accessible and interchangeable by creating a skeleton that would allow the components to be clicked into place. This skeleton would contain parts which would be form fitted to the size of each component, making it easier to swap out. Similar to how the surrogate UUV was created to be transport between multiple vehicles, creating a skeleton for interchangeable components would allow users to only replace components that needs to be changed, rather than the entire system. 3D printing would be a good choice since the fill density can be changed and it can also print very specific dimensions down to a fraction of a millimeter (depending on the printer).

5.2.8 Scaled HPS Vehicle

Though one of the goals is to implement the surrogate UUV into the human-powered submarine, it would be useful to construct a scaled version on the surrogate. It would have the control surfaces of The Underdawg at the same locations on the surrogate and be its own standalone system. With this, smaller scale testing can be done without needing the human-powered submarine and the additional crew members that are generally required for testing.

5.2.9 HPS Implementation

The surrogate UUV implementation in The Underdawg, the human-powered submarine at UW, will entail choosing a location for the system to be fixed. Since the system will be measuring position and orientation, the fixed location is required to be at the same center of gravity and buoyancy in both the x- and y-direction of the vehicle. Otherwise, further calculations would be required to account for addition orientation changes. The Underdawg will be filled with water as it descends further into the water, however, that should not be an issue since the attitude control system

is built inside a watertight container. We do need to ensure there are no leakage for our system prior to any underwater testing.

5.2.10 Underwater HPS Testing

Subsequent to the HPS implementation, there are two underwater testing phases. First is a stationary test to ensure the position and orientation from the sensor output remains the same for the duration of the test. Once that is complete, testing the vehicle moving underwater and watching for any discontinuities between signals, including the time until it is reconnected. Since water may affect the connectivity of the Bluetooth, it would be appropriate to see the extent of the connectivity range.

5.2.11 Adding GPU

Though the system is created to work in real-time, we can further advance the system by adding a graphics processing unit (GPU). The GPU is meant to increase memory manipulation and accelerate the image creations which would be outputted to the computer. This could also include adding video rendering in real-time.

5.2.12 Live CAD Model

With the outputted sensor going to the computer, it would also be useful to have a live CAD model, demonstration its current orientation and actuator movements based on the signal processed. Since we are unable to see the vehicle underwater, adding a CAD model rendering on the computer would provide additional visual representation on the vehicle itself.

5.2.13 Change In Buoyancy

As mentioned in Chapter 2, the human-powered submarines at UW from past to present are all positively buoyant. This makes it so the vehicle tilts downward toward

the bow. Though it makes it so the vehicle remains in the water, this increases the work necessary to traverse from one point to the next. By making the human-powered submarine neutrally buoyant, it would also make it easier on the attitude controller.

5.2.14 Moving Mass

Keep in mind that the current system is simplified, meaning there are additional calculations that can be integrated to enhance the overall system. Since there is a human pilot manually controlling part of the human-powered submarine, we can assume that there will be changes to the center of gravity (CG) and center of buoyancy (CB). Therefore, it would be helpful to devise some sort of calculation to incorporate the CG and CB changes based on the pilot's size and movement. More advanced, we can implement moving mass calculations for each pilot to ensure a more accurate output.

5.2.15 Addition Gravity Calculation

We know that gravity will always be pointing down towards the center of the Earth. In return, this affects all mass on Earth, including the human-powered submarine. We can integrate a more detailed gravity calculation adding to the forward movement the vehicle is currently experiencing, especially since since we know the vehicles are all positively buoyant. Though the change is small, this gravity calculation adds to a small adjustment in both the x- and z-direction.

5.2.16 Quaternions

The current system utilizes Euler angles to describe the orientation of the vehicle. In comparison to quaternions, Euler angles are simpler and intuitive, making it easier for simple control and analysis. Though the math may be more complicated, implementing quaternions as an additional output would avid the gimbal lock issue and

can further increase tracking accuracy with its additional degree of freedom.

5.2.17 More Advanced Controller Test

To further enhance the controller we currently have, additional research may be conducted. We can assume the pilot as a closed-loop system and treat human as a pure disturbance. In addition, we can compare the response time between the controller and the pilot, and see how it changes the entire vehicle as a whole. We can also assume for the pilot to act as a delay, so with a pilot induced system, we can run simulations between the controller versus the pilot speed.

5.2.18 Open Waters

Aside from human-powered submarine competitions that may potentially be in open waters, we also assume the system to eventually be integrated into other underwater vehicles that would go into open waters. Outside of the controlled environment of the pool, we also have to account for temperature changes, which may refrain the vehicle controls to work properly. By integrating temperature calculations into the system, we can account for changes in the controls, and make prepare a solution in advance. The current calculations in MATLAB Simulink does provide disturbance calculations, it only assumes wave and other water disturbance as a set value, and has not been tested yet. For the open waters, it would be good to research further into the water disturbance and how it would affect the vehicle. The hope for this project is for it to eventually to be on a larger scale (as shown in Fig.5.2).

BIBLIOGRAPHY

[1] N. R. Hussey and C. P. Brancart, "The international submarine races (isr) the first 19 years plus the next 19 years and beyond," *OCEANS*, pp. 1–8, 2008. DOI: https://doi.org/10.1109/OCEANS.2008.5289432.

[2] C. Yates, *Tradition with a modern twist*, Available at https://www.me.washington.edu/news/2017/11/08/tradition-modern-twist (2017/11/08).

[3] M. Gertler and G. R. Hagen, "Standard equations of motion for submarine simulation," *TRID*, vol. SR 009 01 01, no. Task 0102, pp. 1–42, 1967. DOI: http://dx.doi.org/10.1002/andp.19053221004.

[4] J. F. Peter Ridley and P. Corke, "Submarine automatic control," *Proc. Australian Conf. Robotics and Automation*, pp. 1–6, 2003.

[5] H. Ghassemi and E. Yari, "The added mass coefficient computation of sphere, ellipsoid and marine propellers using boundary element method," *Polish Maritime Research*, vol. 18, no. 1, pp. 17–26, 2011. DOI: http://dx.doi.org/?.

[6] J. Severholt, "Generic 6-dof added mass formulation for arbitrary underwater vehicles based on existing semi-empirical methods," PhD thesis, Sweden, 2017.

[7] J. Bennet, *The preposterous world of human-powered submarine racing*, Available at https://www.popularmechanics.com/technology/infrastructure/a27474/human-powered-submarine-racing/ (2017/08/09).

[8] T. I. Fossen, *Handbook of Marine Craft Hydrodynamics and Motion Control*. United Kingdom: John Wiley Sons Ltd., 2011.

[9] "A six degree of freedom model for a submersible," pp. 1–16, DOI: https://core.ac.uk/reader/15718.

[10] V. Cusati, "A comprehensive review of vertical tail design," *6th Symposium on Collaboration in Aircraft Design*, pp. 1–15, 2016. DOI: http://dx.doi.org/10.13140/RG.2.2.12606.69448.

[11] N. E. Leonard and J. G. Graver, "Model-based feedback control of autonomous underwater gliders," *IEEE Journal of Oceanic Engineering*, vol. 24, no. 4, pp. 633–645, 2001. DOI: https://doi.org/10.1109/48.972106.

[12] S. D. Kadam and K. N. Tiwari, "A simplified approach to tune pd controller for the depth control of an autonomous underwater vehicle," *Communication, Computing and Networking Technologies*, no. 5, pp. 209–212, 2013.

[13] E. Y. Hong and M. C. Abstract, "Roll control of an autonomous underwater vehicle using an internal rolling mass," *Annalen der Physik*, vol. 105, pp. 229–242, 2015. DOI: http://dx.doi.org/10.1007/978-3-319-07488-7_16.

[14] E. Gouthami and M. A. Rani, "Modeling of an adaptive controller for an aircraft roll control system using pid , fuzzy-pid and genetic algorithm," *IOSR Journal of Electronics and Communication Engineering (IOSR-JECE)*, vol. 11, no. 1, pp. 15–24, 2016.

[15] U. C. Università, "Real-time simulation of a cogag naval ship propulsion system integration of numerical modeling and simulation techniques for the analysis of towing operations of cargo ships," *International Review of Mechanical Engineering (I.RE.M.E.)*, vol. 7, no. 7, pp. 1–11, 2013. DOI: http://dx.doi.org/10.1243/14750902JEME121.

[16] W. Lin, "Hybrid intelligent control for submarine stabilization," *International Journal of Advanced Robotic Systems (IJARS)*, vol. 10, no. 221, pp. 1–11, 2012. DOI: http://dx.doi.org/10.5772/56392.

[17] H. M. Alzu'Bi and B. Sababha, "Model-based control of a fully autonomous quadrotor uav," *AIAA Infotech at Aerospace (I at A) Conference*, pp. 1–6, 2013. DOI: http://dx.doi.org/10.2514/6.2013-5136.

[18] U. W. HPS, "The underdawg design report," UW HPS Final Report, 2019-2020.

[19] ——, "The underdawg critical design review," CDR, 2019-2020.

[20] S. L. Nenad Popovich and N. Garimella, "Submarine depth control," *3rd WSEAS/IASME Int. Conf. on Electroscience Technology For Naval Engineering*, pp. 1–5, 2016.

[21] A. S. A. Widyawardana Adiprawita and J. Semibiring, "Unmanned aerial vehicle instrumentation for rapid aerial photo system," *International Conference on Intelligent Unmanned Systems (ICIUS)*, pp. 111–118, 2008.

[22] ([Logitech F310 Wired PC Gamepad]. 2020), [Online]. Available: https://www.ebgames.com.au.

[23] ([Logitech F310 Gamepad]. 2020), [Online]. Available: https://www.target.com.

[24] ([Watertight Enclosure for ROV/AUV (4 Series)]. 2020), [Online]. Available: https://bluerobotics.com/store/watertight-enclosures/4-series/wte4-asm-r1/.

[25] ([Diagram of the watertight enclosure components]. 2020), [Online]. Available: https://bluerobotics.com/store/watertight-enclosures/4-series/wte4-asm-r1/.